

Source–sink turbulence in a stratified fluid

By **B. M. BOUBNOV**[†], **S. B. DALZIEL** AND **P. F. LINDEN**

Department of Applied Mathematics and Theoretical Physics, University of Cambridge,
Silver Street, Cambridge CB3 9EW, UK

(Received 10 December 1992 and in revised form 26 August 1993)

A new method of generating turbulence in a stratified fluid is presented. The flow is forced by a symmetric array of sources and sinks placed around the perimeter of a tank containing stratified fluid. The sources and sinks are located in a horizontal plane and the flow from the sources is directed horizontally, so that fluid is withdrawn from and re-injected at its neutral density level with some horizontal momentum. The sources and sinks are arranged so that no net impulse or angular momentum is imparted to the flow. Measurements of the mixing produced by the turbulence are made using a conductivity probe to record the vertical density profile. The flow field is measured by tracking small neutrally buoyant particles which are placed within the fluid. The tracking of the particles and analysis of the flow fields are done automatically using DigImage, a recently developed suite of particle tracking software. The characteristics of the flow are found to depend on the forcing parameter $F = V/Nd$, where V is the mean velocity of the flow through the source orifices, d is the diameter of the sources and sinks and N is the buoyancy frequency of the stratification. At large F three-dimensional turbulence is produced within a mixed layer centred on the level of the sources and sinks. A comparison of mixing rates measured in this and more conventional experiments is made, and it is concluded that in terms of the local turbulence parameters the entrainment rates are similar. At low F , no significant mixing occurs and the flow is approximately two-dimensional with very small vertical velocities. Under these circumstances a qualitative change in the characteristics of the flow occurs after the experiment has been running for some hours. It is observed that the scale of the motion increases until there is an accumulation of the energy at the largest scale that can be accommodated within the tank. The structure of this large-scale circulation is analysed and it is found that a form of vorticity expulsion from the interior of the circulation has occurred. These results are compared with numerical simulations of two-dimensional turbulence, and some measurements of turbulent decay are discussed.

1. Introduction

The effect of stable density stratification on turbulent flow is to reduce vertical motion and to produce quasi-horizontal flow far from the source of the turbulence. This process is often referred to as the ‘collapse’ of turbulence in a stratified fluid as, for example, when it is applied to the wake behind a moving body, and it is often associated with damping of the turbulence and the end of vertical mixing. Nevertheless, at this stage there is still significant energy in the flow and it is the dynamics of these horizontal motions that are of interest here.

[†] Permanent address: Institute of Atmospheric Physics, Moscow

In the two largest stratified systems on Earth, the atmosphere and the oceans, mesoscale eddy motions take the form of quasi-horizontal recirculating regions of large diameter-to-height aspect ratio. For example, mesoscale eddies in the ocean have typical diameters of 100 km and vertical scales of 2 km. On these scales the eddies are also influenced by the rotation of the Earth, but for the moment we shall concentrate on the effects of stratification.

A further reason for studying turbulence in a stratified fluid is that it is a paradigm for two-dimensional turbulence which has been the subject of many theoretical and numerical investigations. The most striking feature of two-dimensional flows at high Reynolds numbers is the 'inverse cascade' of energy to large scales. This accumulation of energy at large scales results from the inability of vertical vortex lines to be stretched, and manifests itself as an organization of the flow into coherent vortices, as has been beautifully demonstrated by the numerical calculations of McWilliams (1984), Legras, Santangelo & Benzi (1988), Dritschel (1993) and others. And, since energy does not cascade to small scales where it can be dissipated by viscosity, rates of decay of the motion are small. Thus these coherent structures are persistent features of the flow.

This paper describes experiments designed to investigate the formation and properties of these structures in a stratified flow. Much of the experimental work on turbulence in stratified fluids has involved the generation of three-dimensional motion, for example by flow through a grid, and has examined the decay, either temporally, or spatially from the generation event. This work has concentrated on the decay process and on the mixing that is produced. The literature on this topic is vast and a recent review and bibliography can be found in Fernando (1991).

The present work has a different focus, in that we have attempted to generate turbulence by providing a horizontal forcing to the flow. In this way we aim to avoid the complications of the transition from a region of fully three-dimensional flow, at least under very stable conditions. The forcing consists of an arrangement of sources and sinks, located in a horizontal plane around the perimeter of a tank containing uniformly stratified fluid (with constant buoyancy frequency). The sources and sinks are directed horizontally, and arranged so that no net angular momentum or impulse are imparted to the fluid. The idea is that fluid is removed at a given level and then re-injected at the same neutral density level with some horizontal momentum. At high injection velocities the jets from the sources are turbulent and cause vertical mixing, but at low injection velocities quasi-two-dimensional motion is produced with very little mixing. Thus these experiments have the capability of producing entrainment into a mixed layer and as such are comparable with experiments in stirring boxes. Additionally, however, they have the capacity to produce horizontal eddies *directly* without there first being a decay of three-dimensional motion. Consequently, we are able to produce flows more similar to numerical simulations of two-dimensional calculations.

The closest related laboratory experiments are those by van Heijst and his co-workers (van Heijst & Flór 1989; Kloosterziel & van Heijst 1991) and by Voropayev (1989). In these experiments the motion resulting from a horizontal jet fired into a stratified fluid is studied. The forcing by the jet has a *finite duration*, and these studies focused on the evolution of structures as the motion decayed after the forcing had ceased. A jet produces an impulse in the fluid, and the flow evolves into a vortex dipole which continually expands in scale as it decays.

Continuously forced flows have been studied by Sommeria (1986) in which vortices are produced by the imposition of an electric current on a conducting fluid. The flow was constrained to be two-dimensional by the imposition of a magnetic field and

transfer of energy to large scales was observed when dissipation was weak. Colin de Verdiere (1980) examined the motion produced by sources and sinks in a rotating fluid. No inverse energy cascade was observed in that case. We shall return to these experiments in §7.

This paper presents the results of experiments which utilize a recently developed particle tracking system, DigImage, to obtain quantitative data on the velocity fields. We will show that the flow behaves in qualitatively different ways in regimes of high and low stratification, and we shall present quantitative information on the structure of the turbulence. The experimental apparatus and method is described in §2, and the qualitative description of the flow regimes is given in §3. Quantitative results on the vertical mixing are described in §4, and a discussion of the flow structures is given in §5. Measurements of turbulence decay after the forcing was turned off are described in §6. A comparison of our results with other experiments and with numerical calculations is given in §7.

2. The experiments

The experiments were conducted in a rectangular Perspex tank with a square base measuring 450 mm and depth 300 mm. Around the perimeter of the tank a set of eight sources and eight sinks, two of each on each side, were located at mid-depth in a horizontal plane as shown in figure 1. The orifices of the sources and sinks were 4 mm in diameter and were directed horizontally into the tank, normal to the adjacent vertical wall. The locations as shown in figure 1 ensure that no net vertical angular momentum about the centre of the tank nor any net impulse is imparted to the fluid. Each source–sink pair is connected via tubing through eight channels of a variable-speed peristaltic pump, which provides a controllable and equal flow rate from each source.

The tank was filled with stratified salt solution. The stratification was linear and produced by the standard ‘double-bucket’ method. Once the tank was filled the pump was run for a few minutes to clear any air from the tubing connecting the sources and sinks. The density profile was then measured to check that the vertical density gradient was uniform. Seeding particles were added for flow visualization and for the particle tracking, and the system was left for a period (about an hour) to allow any residual motion to die away. The experiment was started by turning on the pump and monitoring the flow over a period of time (often a day). In some cases the decay of the turbulence after the pump was turned off was also observed.

Flow visualization and measurements of the velocity field were obtained from video recordings of the seeding particles placed in the flow. The particles were produced by grinding and sieving Pliolite, an opaque white resin with a density of approximately 1030 kg m^{-3} . By suitable choice of the density gradient the particles can be arranged to be neutrally buoyant at a desired level in the fluid. The particles were illuminated by a planar sheet of light from two slide projectors placed on opposite sides of the tank. For most of the observations a horizontal light sheet 5 mm thick in the plane of the sources and sinks was used, and the flow was observed via a video camera located above the tank. These plan views were supplemented in some cases with elevation views with the light sheet illuminating the vertical mid-plane of the tank.

The video records of the flow were analysed digitally using DigImage, a particle tracking system developed at DAMTP (Dalziel 1993). The system locates the particles on successive video frames and this information allows the characteristics of the flow fields to be determined. Up to 4095 particles are located with subpixel accuracy.

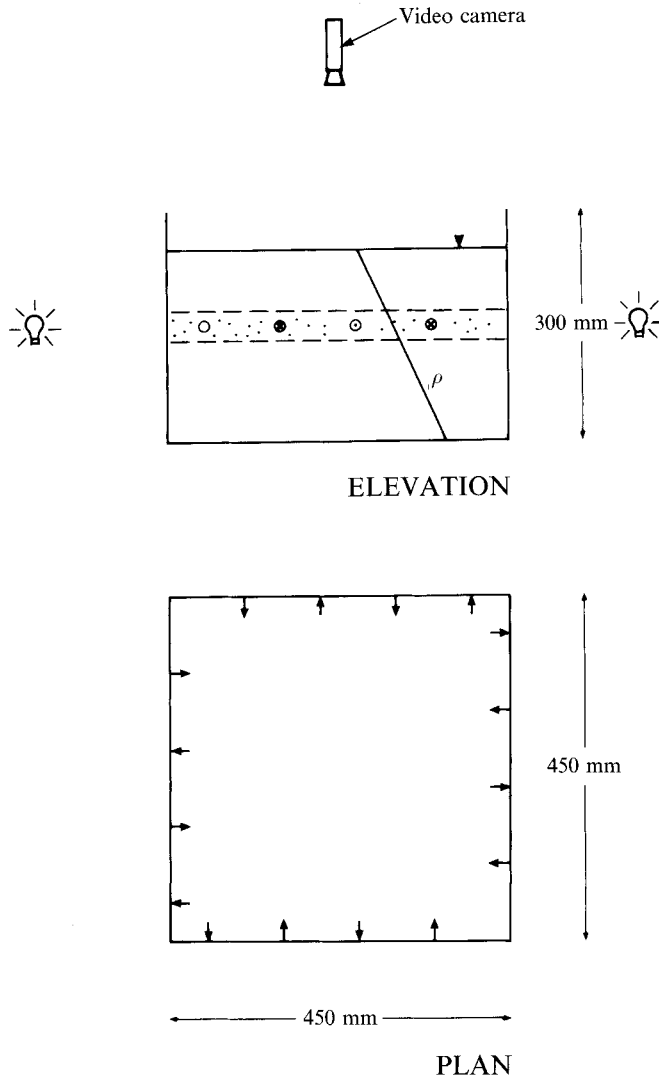


FIGURE 1. A diagram of the experimental apparatus showing the location of the sources and sinks, and the arrangement for measuring particle motions in a horizontal plane. Measurements made in a vertical plane were obtained by interchanging the position of the light sheet and the video camera.

(provided each particle occupies two or more pixels) in each frame of a video sequence. Particles are matched between successive frames in the sequence using information about the particle geometry and, where they are known from previous time steps, the particle velocities. Flow velocities are finally determined by local least-squares fits to the Lagrangian particle paths. In these experiments we used 0.5 mm diameter particles and typically tracked 500 per frame. The system is capable of sampling video frames at 25 Hz, but the flow was sufficiently slow that successive frames at 0.12 s intervals proved to give quite adequate resolution.

Density measurements were made using a calibrated conductivity probe which was traversed to give vertical profiles of density. At high pumping speeds vertical mixing was produced and these records enabled us to measure the mixing rate.

For a given fluid and a given arrangement of sources and sinks there are two

Exp no.	V (cm s^{-1})	N (s^{-1})	F	Re
1	1.4	1.0	3.0	68
5	11.4	1.4	19.7	455
6	5.4	1.6	8.6	215
7	5.4	0.9	14.5	215
8	8.5	1.4	15.4	339
10	2.8	1.4	5.0	110
11	1.4	1.4	2.4	55
12	11.4	2.8	10.0	455
13	8.5	2.1	10.1	339
14	5.4	2.9	4.7	215
15	2.8	3.1	2.2	110
16	5.4	2.6	5.1	339
17	1.4	2.8	1.3	55
18	11.4	1.3	22.5	455
19	8.5	1.2	17.2	339
20	5.4	1.1	12.6	215
21	2.8	1.1	6.4	110
22	1.4	1.0	3.5	55
23	11.4	1.0	28.1	455
24	5.4	1.0	13.1	215
25	5.4	0.9	15.1	215
26	5.4	0.9	14.8	215
27	11.4	0.9	33.1	455
28	11.4	1.8	16.1	455
29	11.4	1.4	19.7	455
30	11.4	1.0	27.3	455
31	11.4	1.3	27.7	455
32	8.5	1.1	19.4	339
33	11.4	1.0	29.0	455
34	5.4	1.0	14.1	215
35	2.8	1.0	7.0	110
36	11.4	1.9	14.9	455

TABLE 1. The experimental parameters. V is the velocity of the jet from each orifice of diameter d , N is the buoyancy frequency, $F = V/Nd$ is the forcing parameter and $Re = Vd/\nu$ is the Reynolds number.

parameters governing the behaviour of the flow. These are the mean velocity V of fluid through the source orifices and the buoyancy frequency $N = [(-g/\rho)(d\rho/dz)]^{1/2}$, where $\rho(z)$ is the density, z is the height and g is the gravitational acceleration. These parameters may be expressed in terms of the two non-dimensional external parameters, the Reynolds number $Re = Vd/\nu$, and the forcing parameter $F = V/Nd$, where d is the diameter of the sources and sinks, and ν is the kinematic viscosity of the fluid. The experiments reported here cover the range $50 \leq Re \leq 450$ and $1 \leq F \leq 33$. The forcing parameter F characterizes the relative strengths of the forcing and the stratification. At low F the stratification inhibits vertical motion and it is expected that the flow will be predominantly horizontal. At higher F the flow from the sources is expected to generate three-dimensional motions and to produce significant vertical mixing. The Reynolds number gives a measure of the strength of viscous forces. Although the values of Re are quite low in these experiments, we shall present evidence to support the assumption that viscous effects are of secondary importance. It should be emphasized that these parameters, although related to, are not the internal Reynolds and Froude numbers of

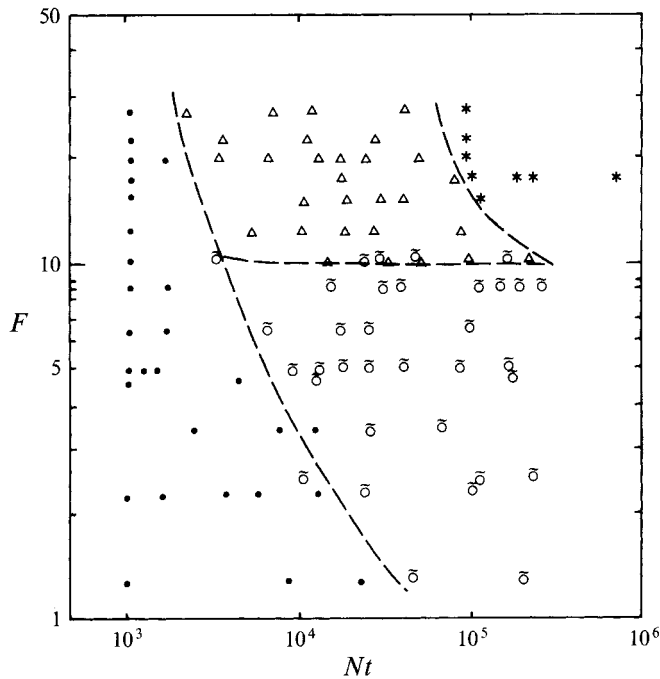


FIGURE 2. The regime diagram for the experiments. Each experiment is plotted according to the forcing parameter F at various dimensionless times Nt during the evolution of the flow. The four regimes are based on visualizations of the flow which have been characterized as: I – vortex interaction (●); II – large-scale circulation (○); III – anisotropic three-dimensional motions (△) and IV – three-dimensional turbulence (★). Examples of the flows in these regimes are shown in figures 3 and 4.

the flow. The relationship between the internal and the external parameters will be discussed in §7. Table 1 gives details of the parameters for each experiment.

3. Flow regimes

The qualitative observations are best summarized by a regime diagram as shown in figure 2. The experiments are plotted in the terms of the forcing parameter F and the dimensionless time Nt , where t is the time measured from the commencement of the forcing. The evolution of any particular experiment can be determined by following a straight line at constant F . The characterization of these regimes is based on observations of the flow patterns and is most easily described by examples from two experiments, exp 18 ($F = 22.5$, $Re = 455$) and exp 21 ($F = 6.4$, $Re = 110$). These two experiments typify the flows at large and small F , respectively, and figures 3 and 4 show examples of the flow patterns at various stages during the evolution of the flow.

Figure 3 shows particle paths obtained from digitized video frames at various times after the pumping started. Each of these views is a plan view in the plane of the forcing, and in figure 3 the streaks show the particles followed for 15 s. The size of the domain shown is 400×375 mm and the orifices of the sources and sinks lie just outside the domain. Figures 3(a) and 3(b) show the flow at early times $Nt = 50$ and 540, respectively, when the flow is in regime I (figure 2). This stage is characterized by approximately horizontal motion as it can be seen from the particle streaks that individual particles stay within the light sheet for long times. There are a number of

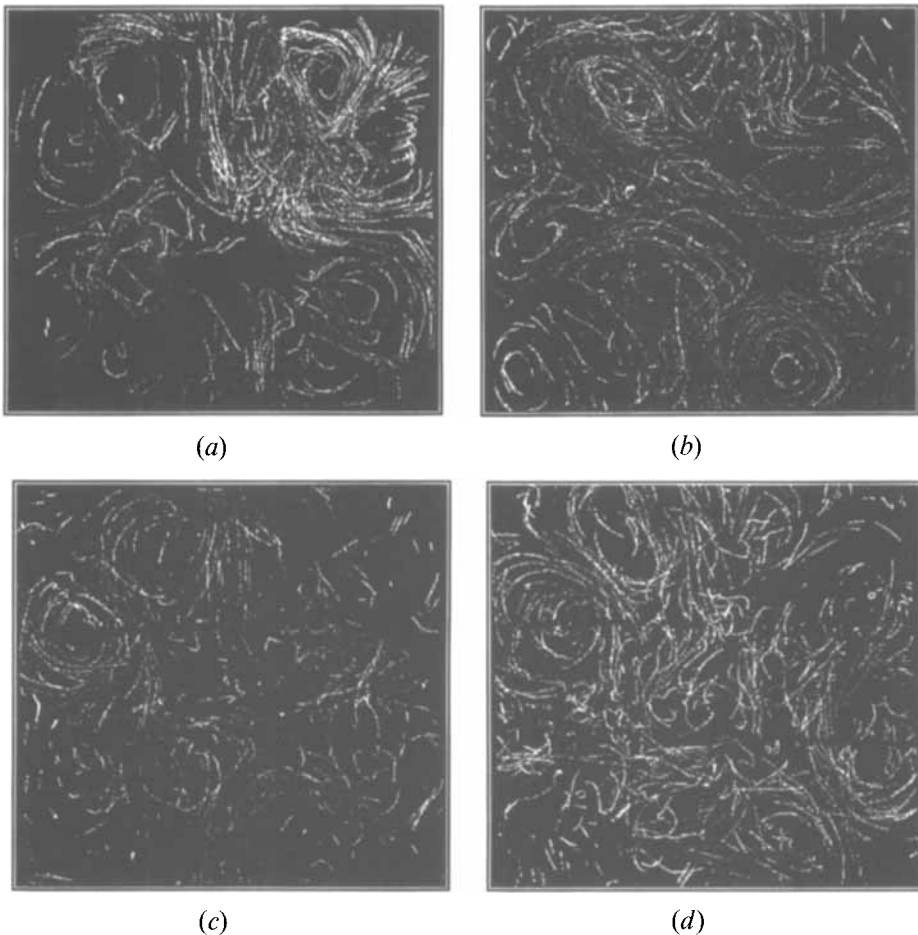


FIGURE 3. Plan-view particle paths in the plane of the sources and sinks for the case $F = 22.5$ and $Re = 455$ (exp 18). The elapsed time for each path is 15 s. The sources and sinks are just outside the domain shown here which measures $400 \text{ mm} \times 375 \text{ mm}$. The non-dimensional times Nt are (a) 50, (b) 540, (c) 2×10^4 and (d) 1×10^5 .

discrete vortices (eight in figure 3*a* and six in figure 3*b*), which are clearly linked to the arrangement of sources and sinks. Some of these vortices, particularly those in the corners of the domain, are persistent features while others vary over quite short timescales apparently as a result of interaction with other vortices. This regime is a consistent feature of all the experiments at early times and we denote it as the ‘vortex interaction’ regime I. Figure 3(*c*) shows the flow at the later time $Nt = 2 \times 10^4$. At this stage the lengths of the particle paths are significantly truncated by the particles leaving the light sheet. This shows that the motion is more three-dimensional than at earlier times, although there remain vestiges of the earlier vortex motion forced by the sources and sinks. This is regime III, called ‘anisotropic three-dimensional motion’. At even later times the motion becomes more three-dimensional, and an example of the flow pattern at $Nt = 1 \times 10^5$ is shown in figure 3(*d*). Even here there is evidence of vortices near the boundaries, but observations of the flow in elevation (see figure 5) show that the flow is fully three-dimensional and we distinguish this regime as IV, ‘three-dimensional turbulence’. This evolution is, of course, associated with modification to the original density profile and the development of significant vertical velocities is

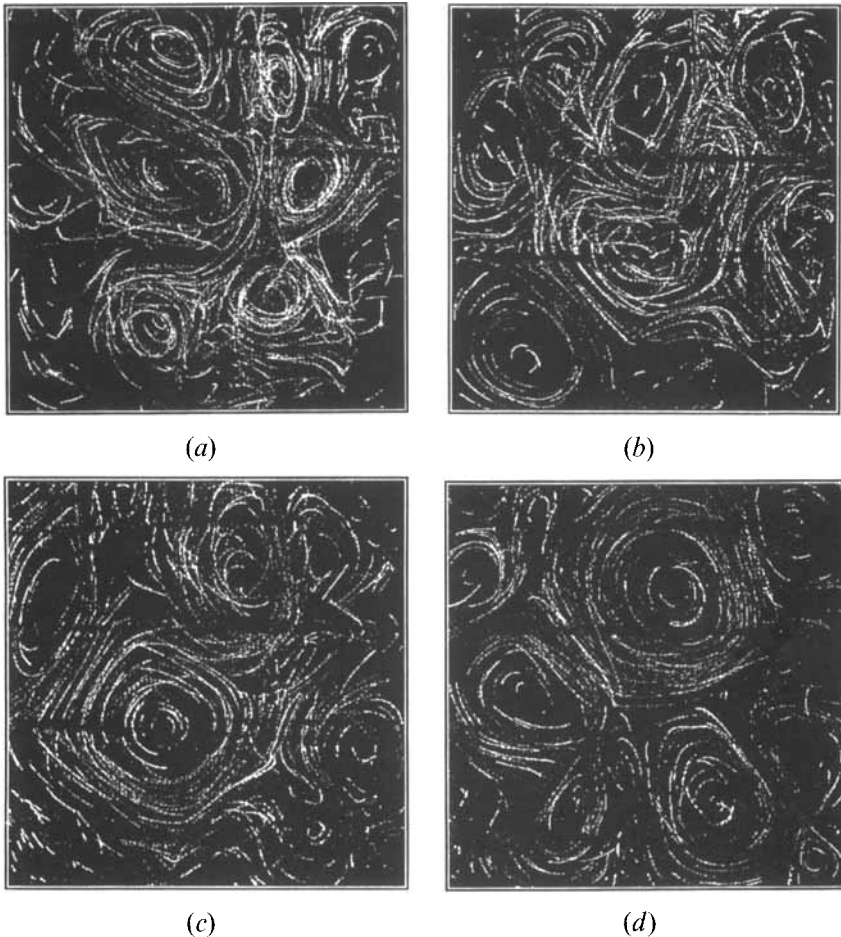


FIGURE 4(a-d). For caption see facing page.

indicative of vertical mixing. We shall return to this point later. The division between regimes III and IV is not clear cut, and we have used elevation views (see e.g. figures 5 and 6) to try to differentiate between them.

The evolution of the flow at low values of the forcing parameter F is quite different, and an example is shown in figure 4 for the case $F = 6.4$, $Re = 110$ (exp 21). At early times $Nt = 180$ and 540 shown in figures 4(a) and 4(b), respectively, the flow is similar in character to that observed in the vortex interaction regime I at large F . While the details of the flow vary, there are several (eight or nine) vortices linked to the arrangement of the sources and sinks. At all values of the forcing parameter examined in these experiments ($F \lesssim 33$), the motion in regime I is primarily horizontal. The stratification inhibits vertical motion and, in the early stages of the experiments, this effect dominates. However, the motion is *not* two-dimensional as there is significant vertical shear which can be seen by the fact that particle paths cross each other (see e.g. figures 4a and 4b). These crossed paths result from particles at different levels in the light sheet and are, therefore, indicative of the vertical shear in the horizontal motion[†]. At later times, at low F , the motion remains horizontal and the vertical shear decreases.

[†] Unsteadiness in the flow can also produce crossed particle paths. However, the timescales for the evolution of the flow are significantly greater than the particle travel time and this effect is negligible.

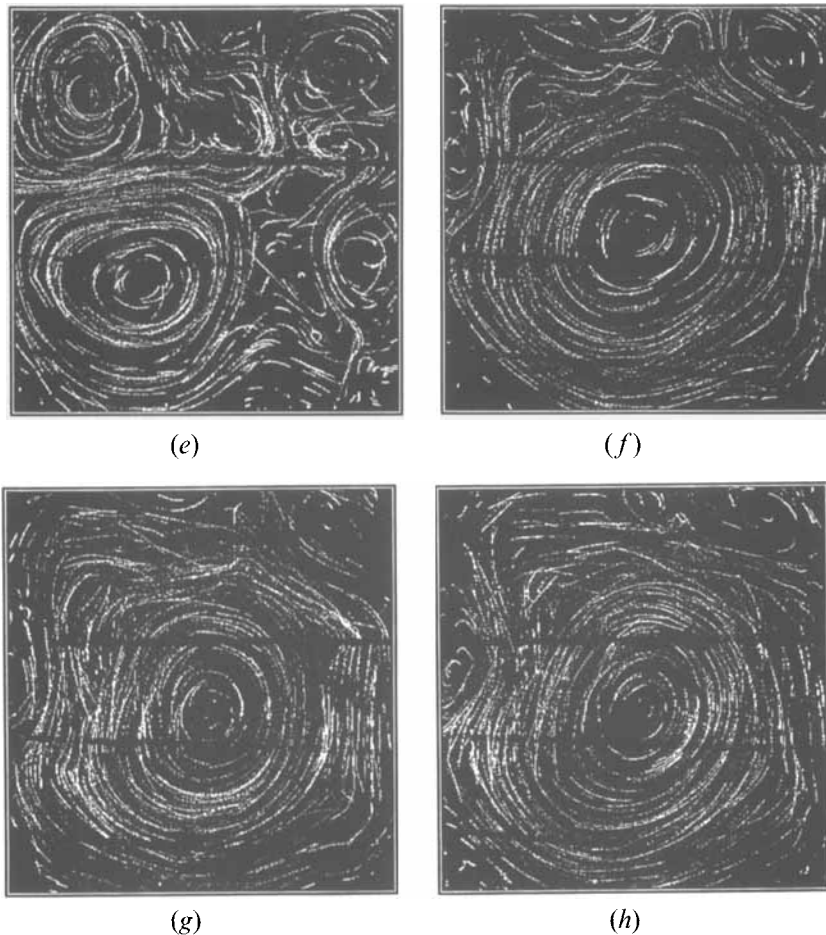


FIGURE 4. Plan-view particle paths in the plane of the sources and sinks for the case $F = 6.4$ and $Re = 110$ (exp 21). The elapsed time for each case is 30 s. The non-dimensional times Nt are (a) 180, (b) 540, (c) 1.5×10^3 , (d) 6×10^3 , (e) 1.7×10^4 , (f) 2.4×10^4 , (g) 7.6×10^4 and (h) 7.8×10^4 .

A comparison of, say, figure 4(d) with figures 4(a) and 4(b) shows that the instances of particle path crossings has reduced significantly. The lengths of the paths remain roughly the same, showing that the flow remains horizontal.

As time progresses the number of vortices decreases and their scale increases slightly, as shown in figures 4(c) at $Nt = 1.5 \times 10^3$, 4(d) at $Nt = 6 \times 10^3$, and 4(e) at $Nt = 1.7 \times 10^4$. At this latter stage the number of vortices has decreased significantly and one or two of these vortices appear to be becoming the dominant features of the flow field. This trend continues and eventually the flow develops a single dominant large-scale circulation as shown on figure 4(f) when $Nt = 2.4 \times 10^4$. This motion is almost completely two-dimensional, as can be seen from the fact that very few of the particle paths cross. Once this circulation is established it remains as the dominant feature, as shown in figures 4(g) and 4(h) at $Nt = 7.6 \times 10^4$ and 7.8×10^4 , respectively. Details of the flow on the perimeter of this circulation change, as a result of the proximity of the sources and sinks, but otherwise the flow pattern and the direction of the flow remain unchanged. This persistence continues over many circulation times. The elapsed time between figures 4(f) and 4(h) is over 13 hours, and this is equivalent to approximately 100 eddy turnover times. We denote this as regime II – ‘large scale

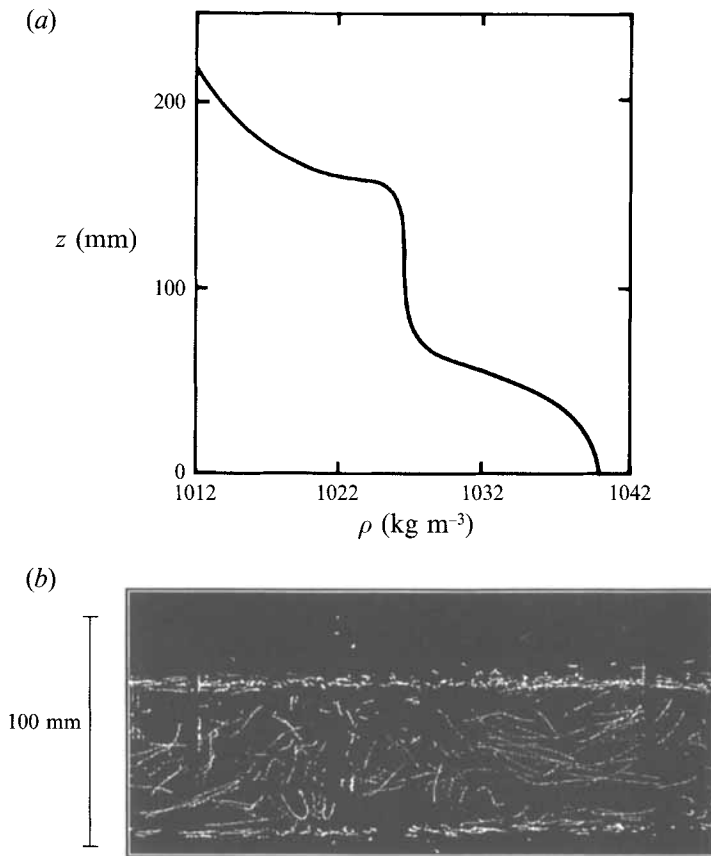


FIGURE 5. The vertical density profile (*a*) and particle paths (*b*) in a vertical plane through the centre of the tank for exp 18 ($F = 22.5$, $Re = 455$) at the time corresponding to the plan view shown in figure 3(*d*). Only a part of the tank is shown in (*b*).

circulation'. As mentioned above, the sign of this circulation does not alter once it is established. Nevertheless, it varies from one experiment to another: for the nine experiments that enter regime II shown in figure 2, the circulation in six is anticlockwise and in three it is clockwise.

Further information about these two flows is given in figures 5 and 6 which show the elevation views of particle motions and vertical density profiles at times corresponding to the last flow patterns shown in figures 3 and 4, respectively. At large F , figure 5(*a*) shows that a significant amount of vertical mixing has taken place and a mixed layer has formed which is centred on the horizontal plane containing the sources and sinks. Above and below the mixed layer the profile approaches the original linear profile, although now modified presumably by molecular diffusion. Within the mixed layer the particle paths show three-dimensional turbulent motion, with a transition to slower, almost horizontal motion at the edges of the stratified region. This density and flow structure is very similar to that observed in other stratified mixing experiments. These results can be contrasted with those at low F shown in figure 6. Although the density gradient at the level of the sources and sinks has been reduced by the flow, a well-developed mixed layer is not formed in this case (see figure 6*a*). The fact that the fluid is stably stratified throughout causes vertical motions to be suppressed as can be seen by the particle paths shown in figure 6(*b*).

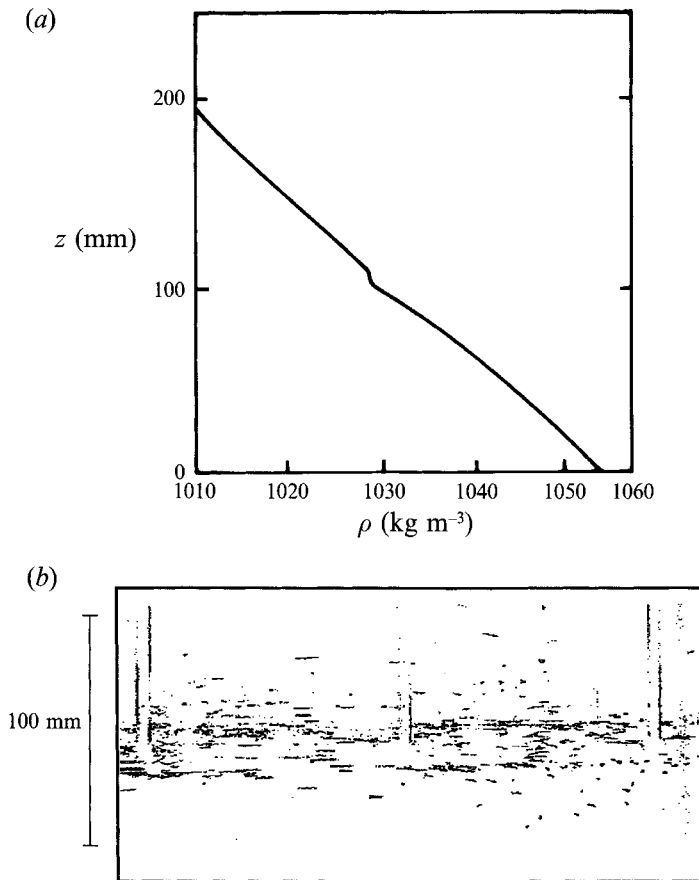


FIGURE 6. The vertical density profile (a) and particle paths (b) in a vertical plane through the centre of the tank for exp 21 ($F = 6.4$, $Re = 110$) at the time corresponding to the plan view shown in figure 4(h). Only a part of the tank is shown in (b).

The time development of the flow depends on the ability of the flow from the sources to 'mix' the stratification. All experiments begin with quasi-horizontal flow in a stable gradient (regime I) and at low F the stratification persists and the flow remains horizontal at all times. The evolution is then towards the largest horizontal scale that can be contained within the tank (regime IV). At high F , vertical mixing occurs and the density gradient near the forcing level weakens. Vertical velocities are less strongly suppressed and the motion becomes three-dimensional (regime III). This motion continues to mix the stratification until a well-mixed layer develops and the motion is fully three-dimensional (regime IV). Further development in these cases is characterized by an increase in the mixed layer depth. The entrainment rate at high F is discussed next.

4. Vertical mixing

As shown in §3, at high values of the forcing parameter F the turbulence generated by the sources is capable of producing a mixed layer, in a manner that appears to be similar to that in other mixing experiments such as stirring boxes. Fluid is entrained from the non-turbulent stratified regions above and below, and the thickness of the mixed layer grows with time. An example of this growth for the case $F = 17.2$

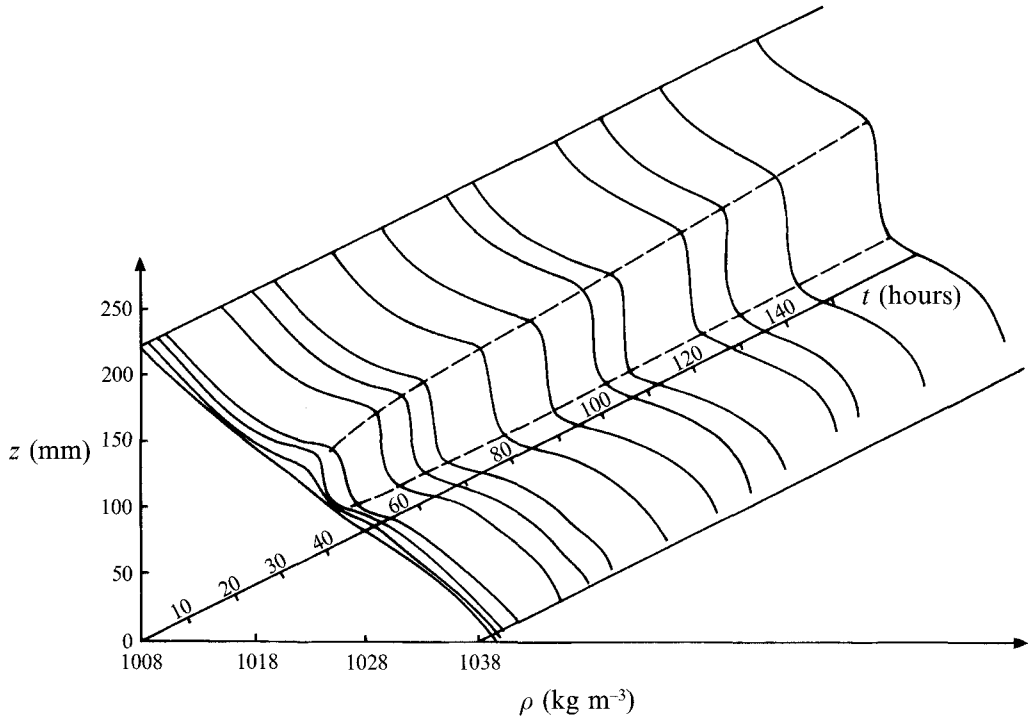


FIGURE 7. The development of the mixed layer, recorded by repeated vertical density profiles made with a conductivity probe, for exp 19 ($F = 17.2$, $Re = 339$). The level of the sources and sinks is at 110 mm measured from the base of the tank.

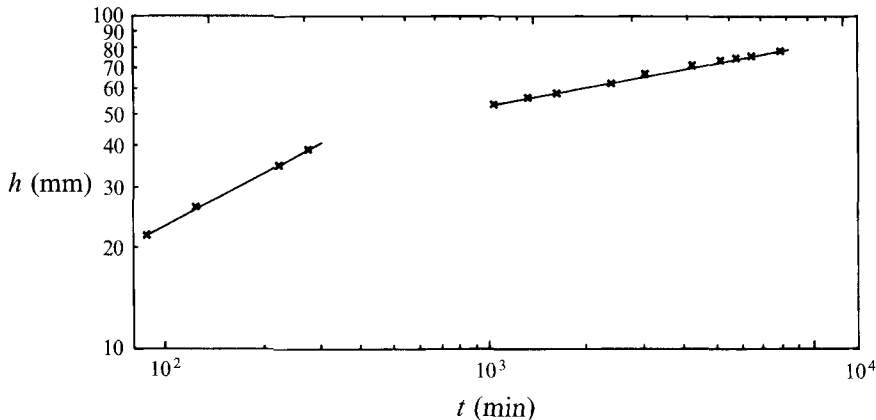


FIGURE 8. The depth h of the mixed layer plotted against time for exp 19 ($F = 17.2$, $Re = 339$). The straight lines through the data are fitted by eye and suggest an initial growth as $t^{\frac{1}{2}}$ and, at later times, as $t^{0.15}$.

$Re = 339$ (exp 19) is shown in figure 7. There is a rapid growth in the mixed layer over an initial period of 10 min or so (not shown in figure 7), which appears to be a response to the initiation of the forcing. Elevation views of the particle motions also support the idea that the early growth is due to the rapid motion induced by the sources and sinks. The stratification weakens during this time as the flow evolves from regime I to regime III (figure 2). A well-mixed layer forms at about $Nt \sim 10^3$ and subsequently the growth

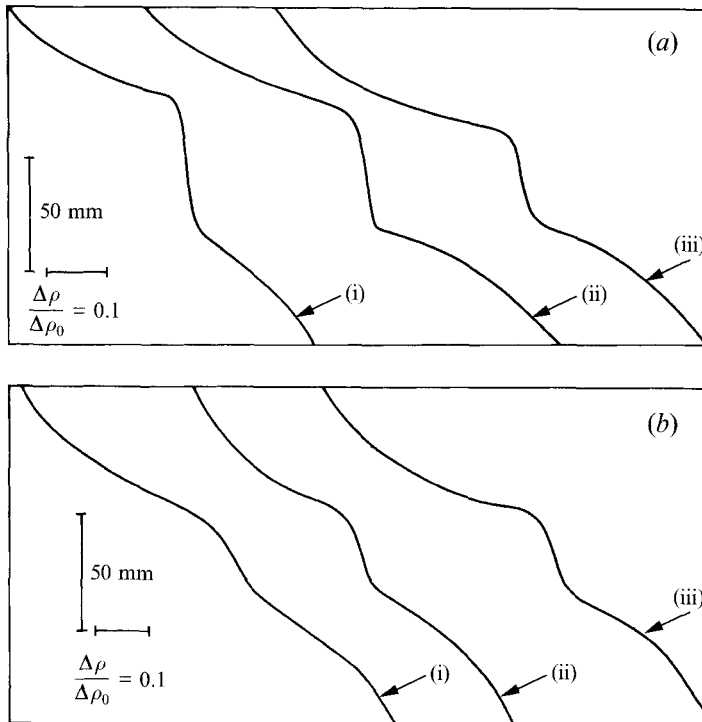


FIGURE 9. Vertical density profiles illustrating the dependence of the mixed layer depth h on the forcing parameter F and the Reynolds number. (a) Profiles at $t = 200$ min at fixed $Re = 445$ for (i) $F = 33.0$, (ii) $F = 19.7$ and (iii) $F = 10.0$. (b) Profiles at $t = 230$ min at fixed $F = 15$ for (i) $Re = 215$, (ii) $Re = 339$ and (iii) $Re = 455$.

continues at a much slower rate. The transition to regime III occurs when the mixed layer depth is approximately 50 mm, which is comparable to the radius of the vortices as determined from the plan view particle paths. The depth h of the mixed layer for exp 19 determined from these profiles is plotted against time in figure 8. For illustrative purposes straight lines representing power laws $h \propto t^\beta$ have been fitted by eye to the data, and these suggest an initial growth $\beta = 0.5$, followed by a slower growth $\beta = 0.15$ at later times.

The dependence of the mixed layer depth h on the external parameters F and Re is shown in figure 9. Figure 9(a) shows illustrative density profiles at fixed $Re = 445$ and time $t = 200$ min for three values of the forcing parameter $F = 33.0, 19.7$ and 10.0 . The depth of the mixed layer decreases as F decreases, showing that mixing is reduced as the stability of the system increases. The effect of Reynolds number is shown in figure 9(b) where density profiles for fixed $F = 15$ and time $t = 230$ min are plotted for three values $Re = 215, 339$ and 455 . If the 'mixed' layer is identified with the region of reduced density gradient centred on the level of the sources and sinks, then the thickness of this layer is independent of Re . However, it is clear that at the smallest value of Re the layer is not well mixed but instead it has a significant stratification, although weaker than the original density gradient in the tank. Since the experiments were all conducted with salt as the stratifying solute the variation with Re also represents a variation with Péclet number $Pe = Vd/\kappa$, where κ is the molecular diffusivity of salt. Effects of molecular diffusion are seen in the vertical density profiles above and below the mixing region shown in figure 9. Diffusion smears out the density steps at the edges of the mixed layer and the profiles return to their original gradients

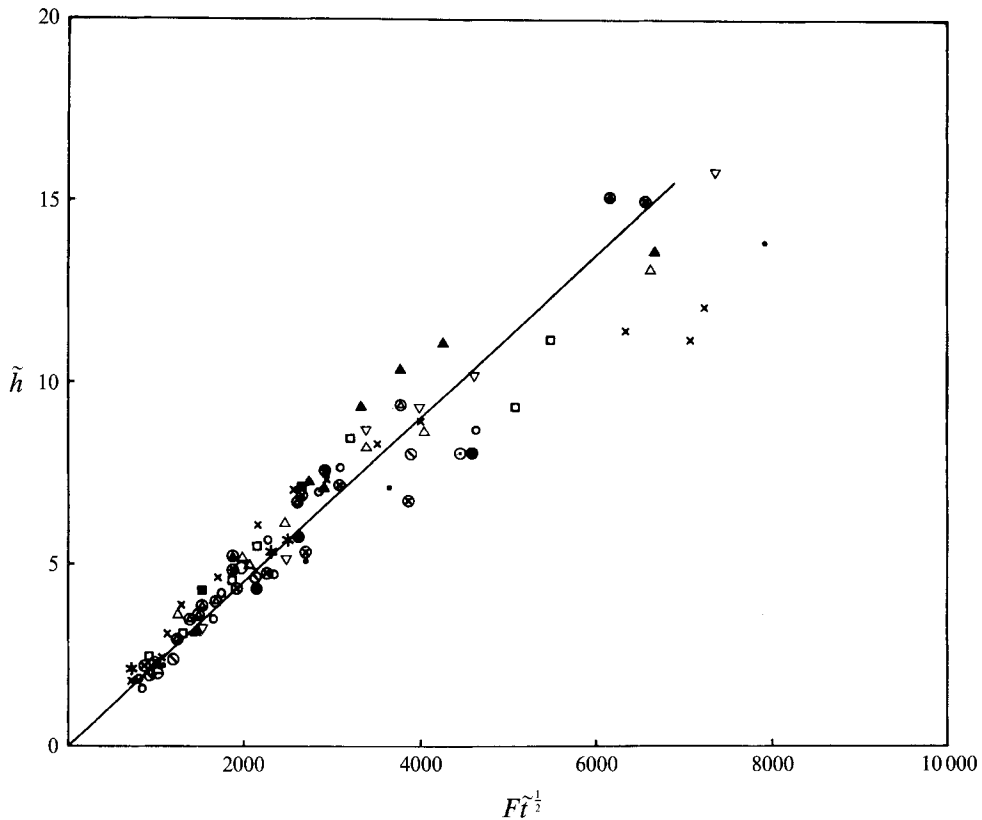


FIGURE 10. The dimensionless mixed layer depth $\tilde{h} = (h - h_0)/d$ plotted against $F\tilde{t}^{1/2}$, where $\tilde{t} = N(t - t_0)$ is the dimensionless time. The experiments with different forcing parameter are indicated by different symbols, and the values of F vary from 10 to 33.

at a distance which grows with time (see also figure 7). It is also clear that the fluid within the mixing zone retains some residual stratification, and that the strength of this stratification increases as the Péclet (Reynolds) number decreases.

For the present discussion we shall call the region of reduced gradient the mixed layer and consider the dependence of the mixed layer growth on the forcing parameter F . As shown in figure 8 and described above, the growth of the mixed layer has two regimes. The data shown there are exceptional as exp 19 was the only experiment that was allowed to continue for such an extended period of time (130 hours). The other experiments in which vertical profiles were measured only exhibited the $t^{3/2}$ growth and, as this time-dependence was observed to be a consistent feature in every case, it is this regime that we now consider further. As mentioned above, we observed an initial development of the mixed layer very soon after the pumping was started. This initial stage appears to be the response to the jets issuing from the sources as the three-dimensional jets collapse. From our observations we have measured the depth h_0 and time t_0 which represents this initial response. Figure 10 plots the subsequent growth of the mixed layer with time. In this figure the dimensionless mixed layer depth $\tilde{h} = (h - h_0)/d$ is plotted against $F\tilde{t}^{1/2}$, where $\tilde{t} = N(t - t_0)$ is the dimensionless time. Minor adjustments have been made to the values of h_0 and t_0 in order that the mean value of the data passes through the origin. The range of F for the 18 experiments shown here is from 10 to 33, and these experiments are those in which three

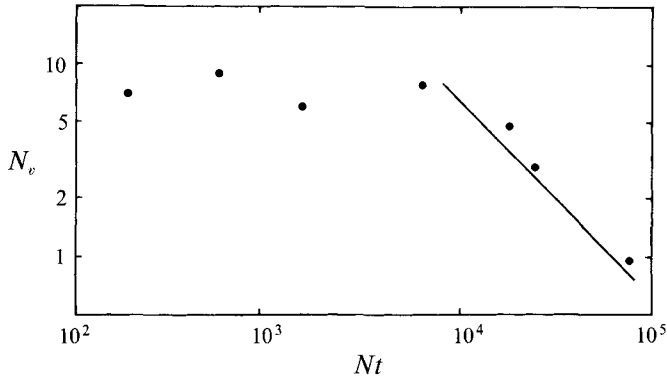


FIGURE 11. The number N_v of vortices plotted against dimensionless time Nt for exp 18 ($F = 6.4$, $Re = 110$). The straight line has slope -1 and is shown for comparison with the data.

dimensional motion is observed (i.e. in regimes I, III and IV shown in figure 2). Experiments at lower F did not develop well-defined mixed layers. Figure 10 shows that much of the data collapse with this scaling, although at later times some of the experiments show lower growth rates. These dimensionless times correspond to about 10^3 min and judging from the data shown in figure 8, it appears that these experiments are entering the lower growth-rate phase exhibited by exp 19. For earlier dimensionless times the data collapse quite well. When the relationship shown in figure 10 is assumed, the entrainment velocity $u_e = dh/dt$ obeys an equation of the form

$$\frac{u_e}{V} = c \frac{V}{Nh}, \quad (4.1)$$

and the experiments give $c = 0.026 \pm 0.008$.

5. Flow structures

The most striking qualitative feature of these experiments is the development of the large-scale circulation at low values of F (see figure 4). As shown in figure 2, this circulation develops over a relatively long timescale $Nt \sim 10^4$ which, for the values of N used in these experiments, corresponds to about 3–4 hours. This slow evolution of the flow is difficult to observe, and so far it has proved to be impossible to determine the exact way in which this circulation develops. The vortices in the flow interact in complicated ways. We have observed instances where vortices of like sign merge and also instances where one vortex will be destroyed by the strain field of a vortex of opposite sign. In these experiments the influence of the jets from the sources extends to the centre of the tank, and in temporarily quiescent regions caused by vortex interactions new vortices will be generated by the continuing flow from the sources. Consequently, individual vortices are destroyed and new ones are formed but the general trend, as illustrated in figure 4, is for the number of vortices to decrease, until a single large-scale circulation remains. When this circulation is established it was observed to persist without change of sign for as long as the experiment was continued.

Figure 11 shows the number of vortices N_v , determined by counting the number of regions of closed particle paths, as a function of the dimensionless time Nt for a low value of the forcing parameter F , exp 18 ($F = 6.4$, $Re = 110$). The number of vortices remains approximately constant until $Nt \sim 10^4$, and then decreases quite rapidly. The

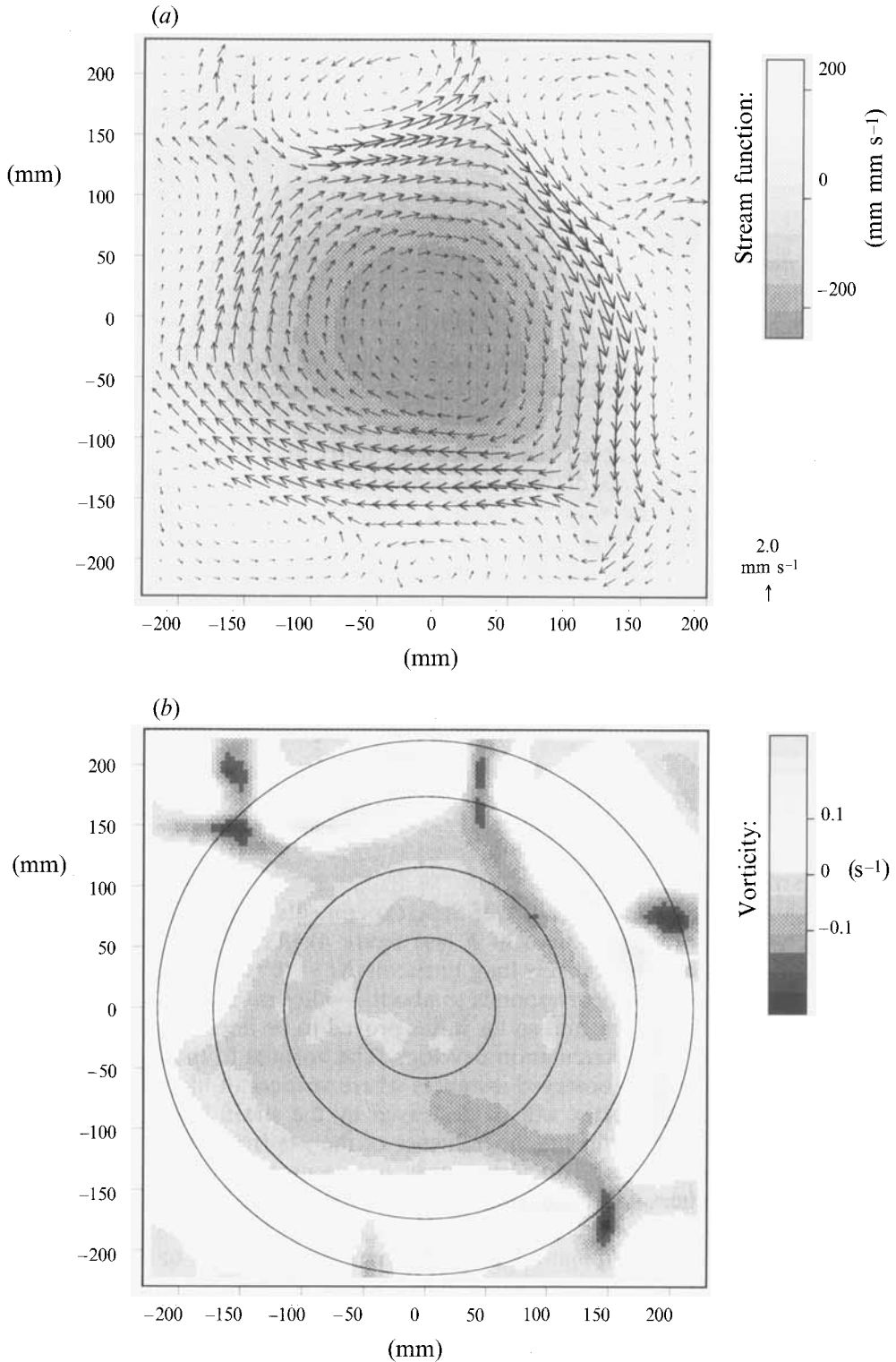


FIGURE 12. The structure of the large-scale circulation for exp 1 ($F = 3.0$, $Re = 68$) measured in a horizontal plane at the level of the sources and sinks. The horizontal velocity field has been mapped onto a regular grid, and this is shown as a vector superimposed on contours of stream function in (a). The vertical vorticity field is shown in (b).

large-scale circulation is established before $Nt \sim 10^5$. The reason for this relatively rapid onset of the large-scale circulation after a long period when, despite vortex interactions, the number of vortices was roughly constant appears to result from the two-dimensionalization of the flow. As was pointed out in §3 in relation to the flow shown in figure 4, while the flow at low F is forced to be horizontal by the stratification, initially it is localized in the plane of the sources and sinks and there is significant vertical shear. At later times, this vertical shear diminishes as the motion penetrates into the stratified fluid above and below the plane of the forcing. Consequently, vertical vortex lines cannot be stretched nor, at later times, can they be twisted and hence the transfer of energy to small scales is inhibited. As pointed out by McWilliams (1990), interactions between pairs of vortices implies that N_v satisfies $dN_v/dt \propto -N_v^2$ and hence $N_v \propto t^{-1}$. A line of slope -1 is plotted in figure 11 and it is not inconsistent with the data for $Nt > 10^4$. However, since there is less than a decade variation in N_v over the course of the experiment, this result must be treated with considerable caution.

The structure of the large-scale circulation is illustrated in figure 12 which shows the velocity over the flow domain mapped onto a regular grid. This experiment (exp 1, $F = 3$, $Re = 68$) was seeded with a larger than usual number of particles and approximately 1500 were tracked, allowing the flow field to be more accurately resolved. The velocities on a regular grid were calculated from the randomly distributed particle paths by fitting bilinear functions at each grid point using a Gaussian weighted-least-squares technique. This technique acts as a weak low-pass filter and provides direct information on the velocity and velocity gradients at each grid point. The vorticity was calculated directly from the velocity gradients while the stream function was evaluated by an iterative integration routine from the velocities. Dalziel (1993) estimates 5% error in the velocities and 10% in the vorticities. The error in the stream function is probably comparable with that in the velocity. The velocity vectors are superimposed on contours of the stream function ψ in figure 12(a) and vertical vorticity ω in figure 12(b). This figure shows that the vorticity gradients are confined to a relatively thin region around the edge of the large eddy, and that the fluid in the centre of the circulation has almost uniform vorticity. The vorticity produced by the sources and sinks, which are still actively pumping, has been expelled from the centre of the flow domain. The contours of vorticity show that the centre of the eddy has a weak negative vorticity and the edges of the circulation are characterized by thin regions of positive vorticity. The inputs from some of the sources can be clearly seen near the boundaries of the domain, and the shape of the large eddy is deformed by these forced eddies.

In a strictly two-dimensional flow with no sources or sinks of vorticity, $\omega = \omega(\psi)$. Figure 13 shows a scatter plot of vorticity and stream function from the flow shown in figure 12. The region at the centre of the large-scale circulation is characterized by the region of fairly constant negative ω at large positive values of ψ . In this part of the flow the values of ω and ψ are quite well correlated, and the motion is close to solid-body rotation. The edges of the circulation are the regions of positive values of ω which occur at smaller values of ψ . Here, there is considerable scatter and the values of ω and ψ are poorly correlated. This scatter is a reflection of the forcing by the jets from the sources where the motion is unsteady, has some weak three-dimensional components and has vertical shear. The area integral of ω over the flow domain is approximately 1% of the peak amplitude of ω . The small value of the integral is consistent with the fact that the net circulation around the boundary is approximately zero.

The departure from the functional relationship $\omega = \omega(\psi)$ is a measure of the

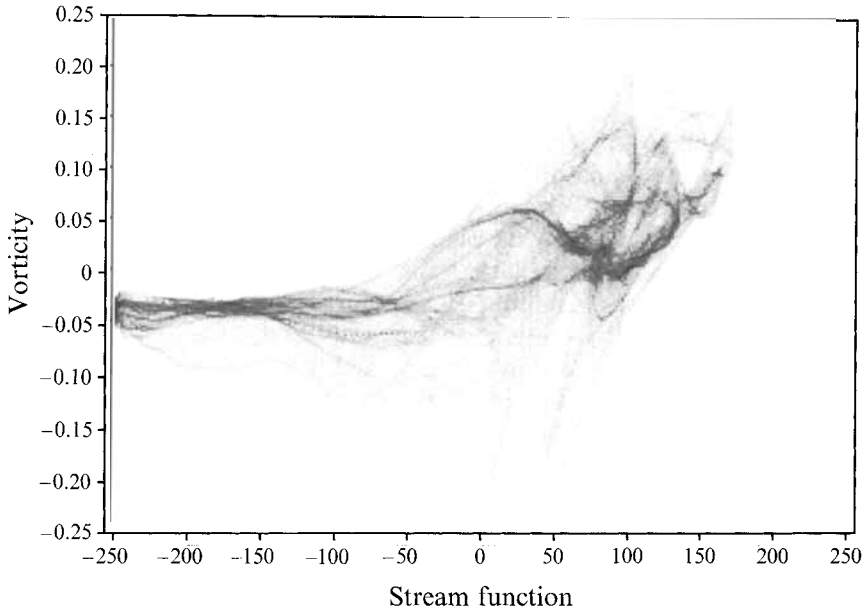


FIGURE 13. A scatter plot of vertical vorticity ω against stream function ψ for the flow shown in figure 12.

deviation from free-mode behaviour. As shown by Read, Rhines & White (1986) the area enclosed by a circuit in (ψ, ω) -space is equal to the net flux of ω out of the corresponding area in physical space. Figure 14 shows trajectories in (ψ, ω) -space corresponding to circular paths in the (x, y) -plane. The circles are centred in the middle of the flow shown in figure 12 and have radii of $r = 0.25$ (a), $r = 0.5$ (b), $r = 0.75$ (c) and $r = 0.95$ (d) ($r = 1$ corresponds to the circle whose tangents form the sides of the tank).

If the circular paths are traced in an anticlockwise direction, then anticlockwise ‘loops’ in the (ψ, ω) -plane correspond to a positive inward flux of vorticity (indicated by vertical cross-hatching), while clockwise ‘loops’ correspond to a negative inward flux (horizontal cross-hatching). The position of the loops relative to the ω -axis indicates whether a positive vorticity flux is an inward movement of positive vorticity, or an outward movement of negative vorticity. The spread of the vorticity providing the flux is important to the dynamics of the region within the path in (x, y) -space. In this two-dimensional flow the extreme values of vorticity within the region are limited by the extreme values of vorticity that has crossed the boundary.

Within the central region of the flow shown in figure 12 the motion is relatively slow with a clockwise rotation. Vertical diffusion of momentum by molecular viscosity necessitates a net inward flux of negative vorticity to maintain this flow. This flux is clearly visible in figures 14(a) and 14(b). The small area and extent of the simply connected loop in figure 14(a) reflects the simple dynamics and limited dissipation associated with the innermost region of the flow. The more complex structure of the loop for $r = 0.5$ (figure 14b) shows three domains of negative vorticity flux and one domain of positive flux. All four domains represent the movement of negative vorticity. The dominance of the negative vorticity flux is essential to maintain the negative circulation in the central region, while the positive flux domain illustrates the more complex nature of the dynamics at the edge of the central region.

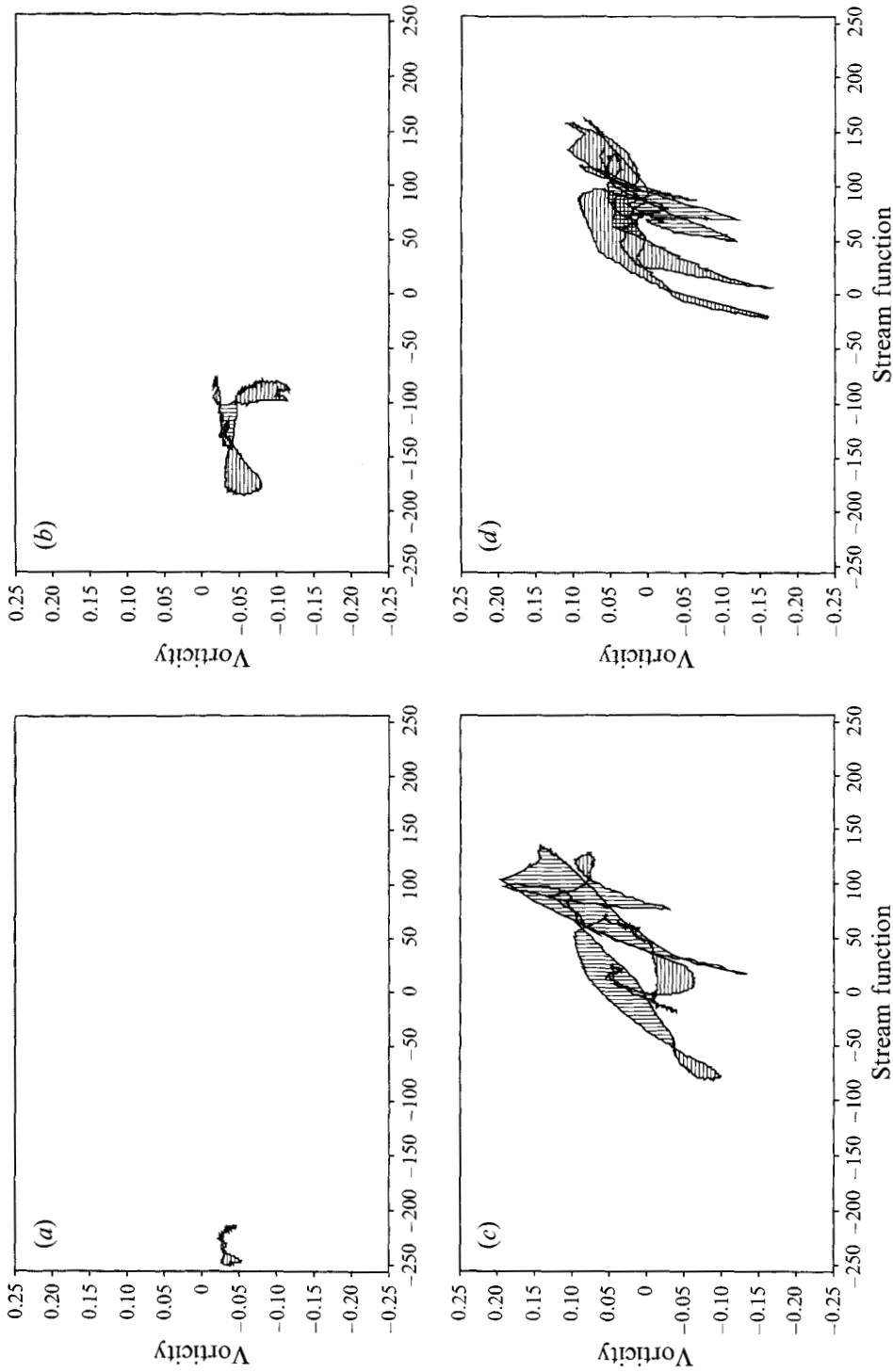


FIGURE 14. Scatter plots in (ψ, ω) -space for the flow shown in figure 12 measured around circles of radius $(a) r = 0.25$, $(b) r = 0.5$, $(c) r = 0.75$ and $(d) r = 0.95$. The circles are centred on the domain shown in figure 12 and $r = 1$ corresponds to the circle tangent to the edges of the domain. The cross-hatching shows the sign of the vorticity flux for the individual loops. A positive flux into the circle is indicated by \equiv and a negative flux by \equiv .

The circle $r = 0.75$ corresponds approximately to the outer edge of the streaming region shown in figure 12, and the values of (ψ, ω) are much more scattered as may be seen in figure 14(c). There is a clear dominance of positive inward vorticity flux across this circle. This flux is provided primarily by the inward movement of positive vorticity and is required to drive the strong streaming region just inside the circle. Most of this positive vorticity is dissipated within this streaming region as can be seen from the dominance of negative vorticity flux across the $r = 0.5$ circle. Regions of the flow with a negative vorticity flux clearly penetrate deeper into the tank in order to drive the flow in the inner regions.

The (ψ, ω) trajectories for the $r = 0.95$ circle (figure 14d) shows a reduced spread in ψ and ω than found for $r = 0.75$. This smaller range of values of ω shows that the outer edges of the flow are unsteady, and more extreme values of ω must have been advected inwards at an earlier time. There is a slight dominance of negative vorticity flux across $r = 0.95$ (the more contorted nature of the trajectories makes a visual comparison of domains of positive and negative vorticity flux more difficult than for the inner circles). This flux is essential to drive the clockwise flow in the inner regions. Reference to figure 12 shows that the four domains where there is strong negative vorticity (two with a positive flux and two with a negative flux) corresponding to positions where the streaming region crosses the $r = 0.95$ circle. Interestingly the positive vorticity extrema are smaller in magnitude, although globally this does not appear to be the case (see figure 13). The larger values of positive ω are found near $r = 0.75$ (figure 14c).

As mentioned above, dissipation through vertical molecular diffusion of momentum requires a continual flux of vorticity to maintain a flow. If this flux is not provided, then the flow will gradually decay with time (see §6). In the case where horizontal molecular diffusion of momentum is negligible (so that there is effectively no diffusion of vorticity across streamlines) compared with vertical diffusion, it is not possible to maintain a region of closed streamlines in a steady state. Figure 12(a) shows clearly that the central region of this flow contains closed streamlines and so it must be unsteady and/or there must be significant horizontal diffusion of momentum. We are able to see unsteady behaviour in these experiments as a gradual changing of the structure of the velocity, vorticity and stream-function fields as regions of more negative vorticity are entrained into the central region. Horizontal diffusion of this vorticity then gradually spreads the vorticity throughout the central region. The diffusion process is enhanced by the relatively high gradients associated with the entrained fluid.

Provided there are no regions of anomalously high horizontal gradients of vorticity away from the regions directly influenced by the flow from the sources, the spread of ω values in the vorticity flux gives an indication of the relative importance of horizontal and vertical diffusion of vorticity. The former is more important when the range of ω values is high, and the latter when it is low. Consequently, we see that in the central region of the flow (figures 14a and 14b) vertical diffusion is more significant than in the outer regions (figures 14c and 14d) where the reduction in the extreme values of vorticity appears to be caused predominantly by horizontal diffusion. An additional energy sink for the more energetic outer region is the generation of internal waves which are subsequently dissipated in the far field. This aspect of the flow has not yet been considered in any detail.

6. Turbulence decay

When the pumping is stopped the decay of the flow to rest depends on the flow regime of the forced flow. Examples of the changes in the structure of the flow for high

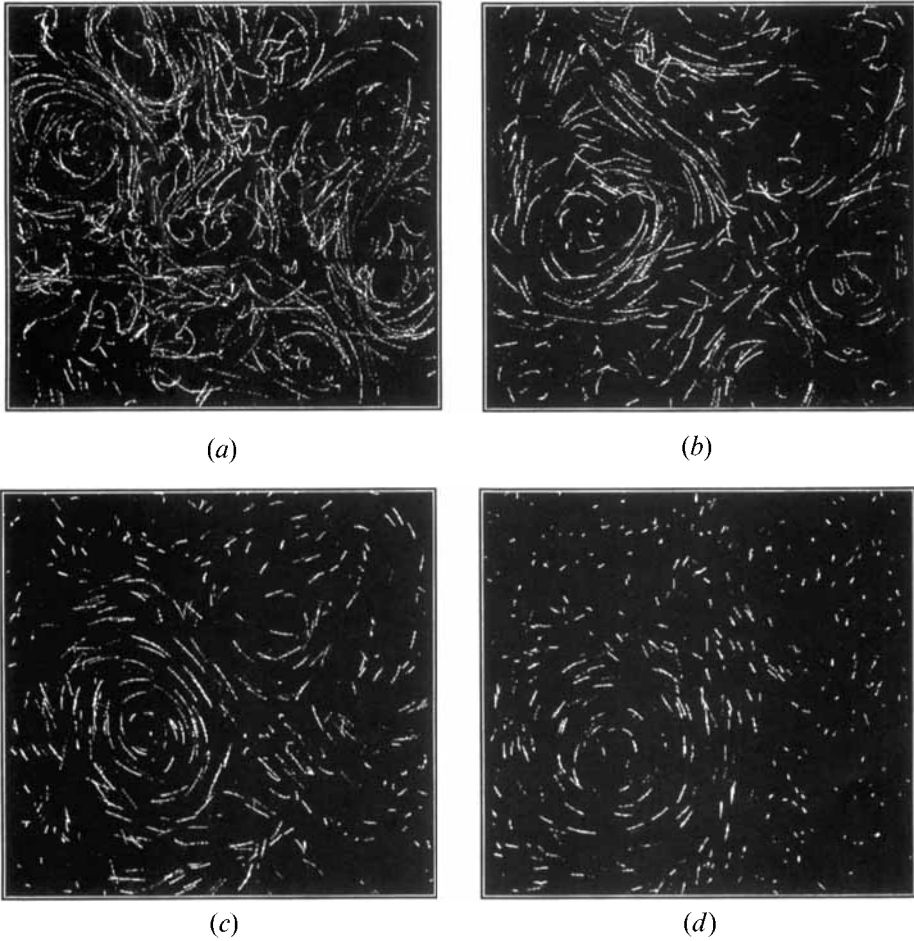


FIGURE 15. Turbulence decay at high F . The example shown is exp 18 with $F = 22$, $Re = 455$. Time t_p is measured from the time the pump is turned off, and the particle paths are shown at dimensionless times Nt_p of (a) 0, (b) 70, (c) 180 and (d) 420.

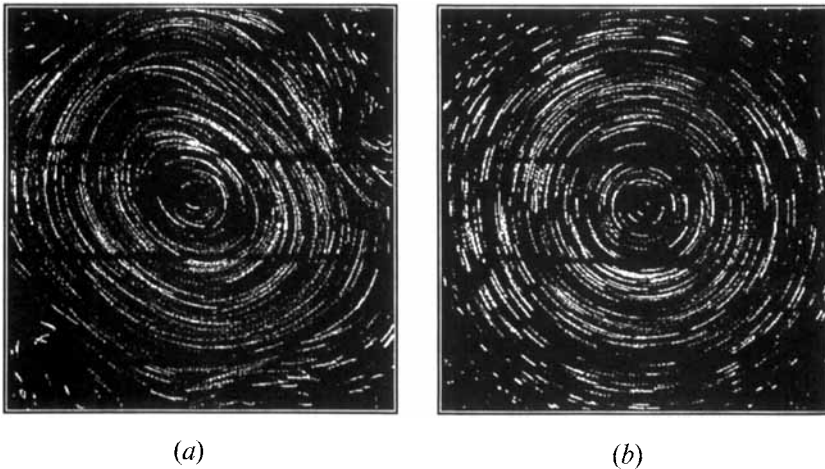


FIGURE 16. Turbulence decay at low F . The example shown is exp 21 with $F = 6.4$, $Re = 110$ at dimensionless times Nt_p of (a) 80 and (b) 130.

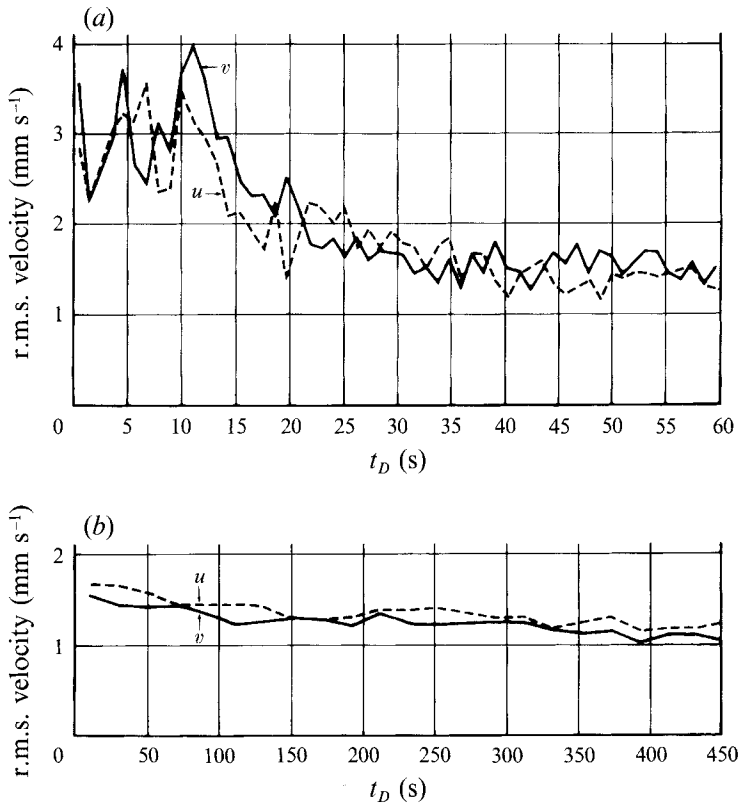


FIGURE 17. The root-mean-square horizontal velocity components u and v plotted against time for (a) exp 19 ($F = 17.2$, $Re = 339$) and (b) exp 20 ($F = 2.6$, $Re = 215$).

and low values of the forcing parameter F (regimes IV and II) are shown in figures 15 and 16. Figure 15 shows the decay of three-dimensional motions at high F for experiment exp 18 ($F = 22$, $Re = 455$) for values of $Nt_D = 0, 70, 180$ and 420 , where t_D is the time measured from the time the pump is switched off. As the motion decays, the lengthscale increases and the flow becomes more two-dimensional. For this experiment the mixed layer is about 50 mm deep when the forcing stops, while the large-scale eddy, which is the residual flow in figure 15(d), measures about 100 mm in diameter. It appears, therefore, since the horizontal scale of the eddy exceeds the vertical scale that this scale of the motion is influenced by the stratification. It is interesting to note that this residual large-scale eddy is visible quite early on in the decay process (see figure 15b) and, although it becomes more axisymmetric and changes its position a little, it remains a robust feature of the flow.

An example of the decay at small F is shown in figure 16, for the case of exp 21 ($F = 6.4$, $Re = 110$) at the dimensionless times $Nt_D = 80$ and 1300 . We see that in this example the large-scale circulation, characteristic of regime II, becomes axisymmetric as the motion decays. This behaviour is typical of all the regime II flows. Note that the motion still remains quite vigorous after the later time, in contrast with the more rapid decay at high F .

The variation in decay rates with F is illustrated in figure 17, where the root-mean-square horizontal velocity averaged over the horizontal flow domain is plotted against time t_D . The two horizontal components u and v are shown for (a) exp 19 ($F = 17.2$, $Re = 339$) and for (b) exp 20 ($F = 2.6$, $Re = 215$). Note that the timescales on the

abscissae of the two graphs are different. This figure shows that the decay is much quicker at high values of F where there is a period of rapid decay followed by a more gradual reduction in the flow velocities. This transition to the slower decay rate corresponds to the two-dimensionalization of the flow noted in figure 15. At low values of F the decay rate is uniformly less, and is not well resolved by these measurements. It is interesting to observe that at later times the two horizontal velocity components are approximately equal throughout the decay of the flow, reflecting the trend of the eddies to become axisymmetric. In the early times, at high F , there are significant fluctuations in the u - and v -components. This variability reflects the three-dimensional nature of the flow at this stage of the experiment.

The time evolution of the large-scale circulation at low F ($F = 6.4$) once the forcing is removed is also illustrated by the stream function ψ and vorticity ω maps and by the (ψ, ω) scatter plots shown in figures 18 and 19, respectively. The forced case corresponding to the particle paths shown in figure 4(*h*) is plotted in figure 18(*a*). At this time the eddy is distorted by the jets and is not exactly circular, and the shape is evolving with time, as may be seen by a comparison between figures 4(*g*) and 4(*h*) which are 25 min apart.

The unforced case is shown in figure 18(*b*) which corresponds to the flow shown in figure 16(*b*) at $Nt_D = 1300$ (about 20 min) after the sources and sinks had been turned off. The plots in figure 18 show the velocity vectors interpolated onto a regular grid and superimposed on the stream-function and vorticity maps. The arrows on the right-hand side and top give the mean x and y velocity components, respectively, averaged along the corresponding line of grid points. The total mean velocity is given by an arrow in the top right-hand corner. This arrow is almost undiscernible in these plots, showing that there is almost no mean flow, as is expected from the arrangement of the sources and sinks.

When the forcing ceases the flow becomes axisymmetric and the regions of high shear at the edges of large circulation dissipate. As figure 18(*b*) shows, the vorticity becomes much more uniform in the freely evolving eddy. This characteristic is also revealed by the (ψ, ω) scatter plots shown in figure 19. The forced case, corresponding to figure 18(*a*), is shown in figure 19(*a*), and the flow after the forcing has been turned off is shown in figure 19(*b*). The range of (ψ, ω) values has decreased as the eddy spins down, but more striking is the reduction in the scatter and the collapse of the values almost onto a single line. The scatter in the forced case is similar to that observed in exp 1 (see figure 13), and much of that was attributed to the time-dependence and fluxes of vorticity from the sources (see figure 14).

When the flow is no longer forced the fluxes of vorticity are removed, and the time-dependence of the flow associated with the viscous decay is weak. Consequently, it is expected that $\omega = \omega(\psi)$ and this relationship is verified by the scatter plot shown in figure 19(*b*). There is a bifurcation in the ω values for points near $\psi = 0$ which corresponds to values for the centre of the eddy and from the boundary of the domain. Otherwise most of the values are consistent with a linear relationship between ω and ψ . Such a relationship is characteristic of a free mode and is similar to that found in other two-dimensional flows (see Kloosterziel & van Heijst 1991).

7. Discussion

We have presented results on the flow generated by an arrangement of sources and sinks placed around the edge of a tank containing stratified fluid. The sources are

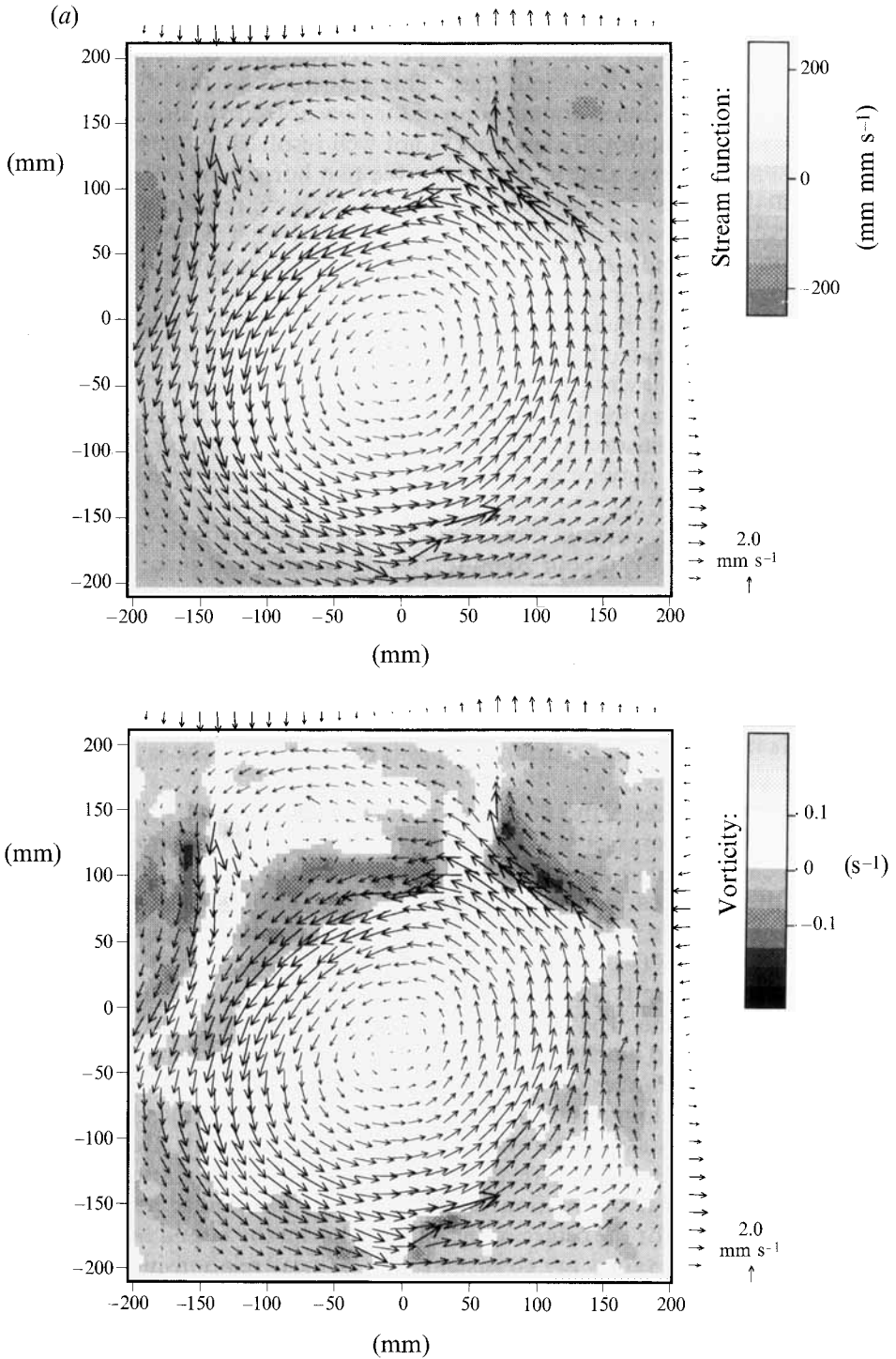


FIGURE 18(a). For caption see facing page.

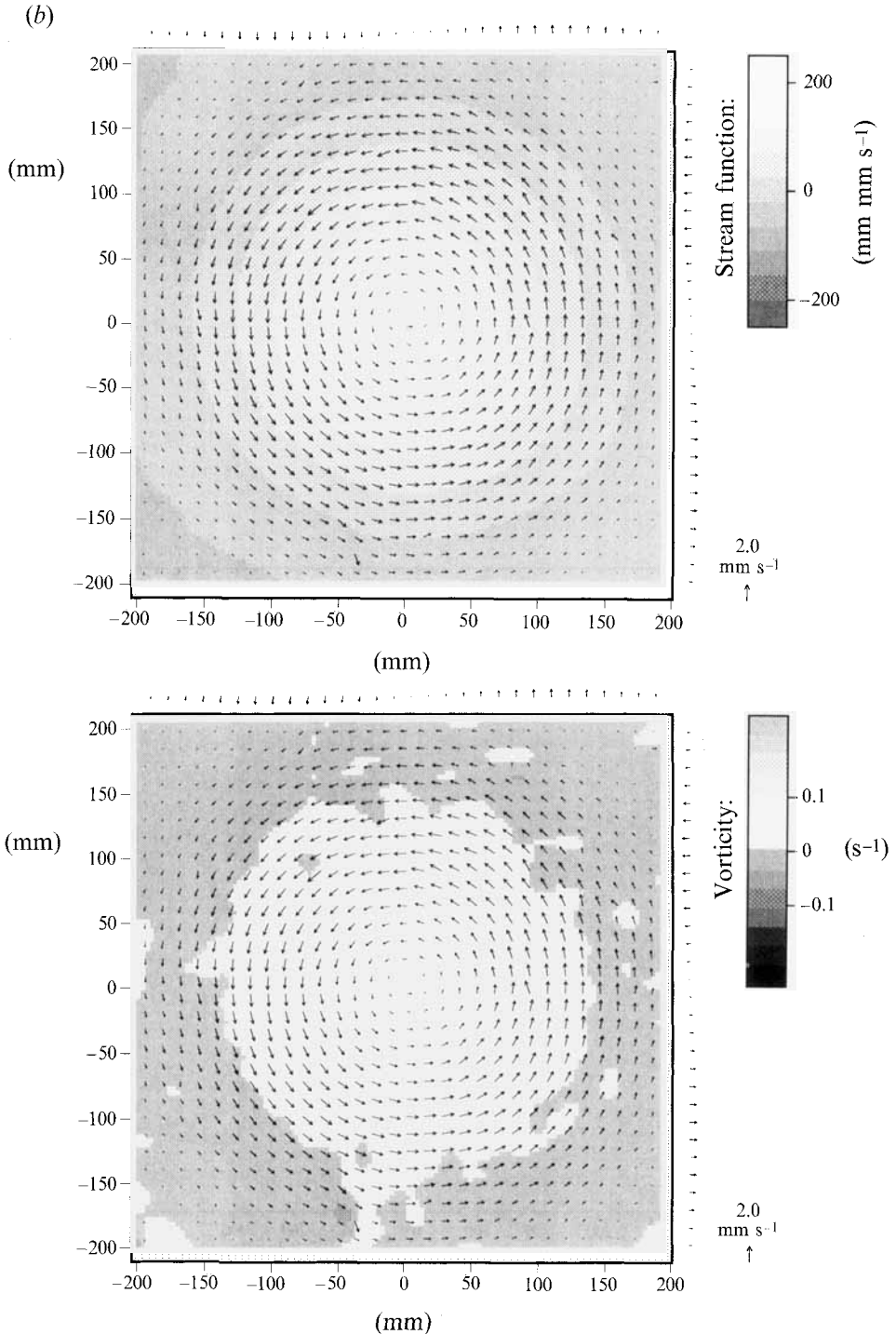


FIGURE 18. Stream-function and vorticity maps for the flow shown in figures 4 and 16. The forced case corresponding to figure 4(*h*) just before the sources are turned off is shown in (*a*), and the unforced case at $Nt_D = 1300$ after the beginning of spindown (figure 16*b*) is shown in (*b*). The velocity field is represented by vectors superimposed on these maps. The mean velocities along horizontal and vertical lines are given by the arrows on the right and above the maps. The total mean velocity is shown by an arrow in the top right-hand corner of each figure. In these cases, the mean velocity is

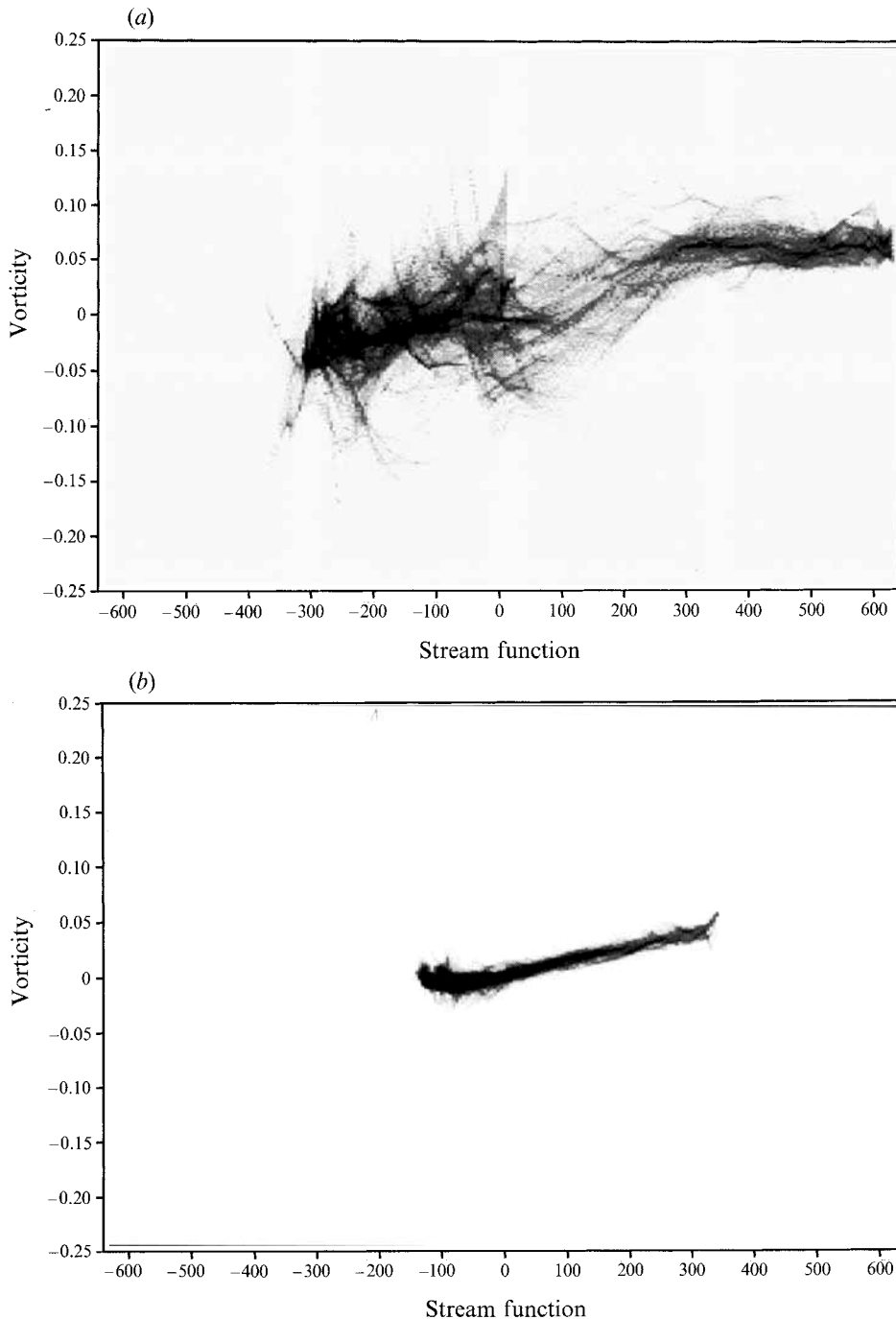


FIGURE 19. Scatter plots in (ψ, ω) -space for the flows shown in figure 18. The forced case is shown in (a) and the unforced case is shown in (b).

located in a horizontal plane so that the fluid is sucked out and replaced at the same (neutral density) level; thus almost no mixing is produced by the pumping mechanism itself. The jets are directed horizontally so that when the pumping rate is low enough there is the possibility of producing nearly two-dimensional motion within the body of

the fluid. At higher pumping rates the jets are sufficiently strong to produce vertical mixing.

Much attention has been paid in the past to the rate of vertical mixing produced by various methods of stirring a stratified fluid. Fernando (1991) has summarized these previous experimental studies, which show that the mixing, which is usually characterized in mixed-layer flows by an entrainment velocity u_e , is a decreasing function of the stability of the system. The exact nature of this functional relationship depends on the way in which the turbulence is generated, and on the structure of the turbulence, particularly near the region where the entrainment of non-turbulent fluid occurs. There is much debate in the literature on this question, and it is not our intention to add to it here. Part of the debate stems from the fact that it is very hard to make unambiguous measurements. Plots of mixed-layer depth versus time are plotted on logarithmic axes and fitted with virtual origins, which make determination of u_e from the slopes of such plots an uncertain process. Our results shown in figure 10 suffer from the same uncertainties, as can be seen from the scatter in the data. However, it is instructive to make some comparison of our results with these other studies.

The relationship (4.1) between u_e and the external parameters can be rewritten in terms of the internal flow variables by noting that the root-mean-square horizontal velocity u was measured as a function of the jet speed V and found to obey a linear relationship of the form

$$u = 0.13V. \quad (7.1)$$

If we assume that the integral scale l is proportional to the mixed layer depth h of the turbulence with a value $l \sim 0.5h$, then (4.1) may be written as

$$u_e/u \sim 0.7(u/Nl). \quad (7.2)$$

Using the usual Richardson number $Ri = N^2 l^2 / u^2$ to measure the stability of the flow, (7.2) implies that the dimensionless entrainment rate is proportional to $Ri^{-\frac{1}{2}}$, which is a weaker dependence on stability than is observed in grid-stirred tanks (E & Hopfinger 1986; Nokes 1988). The constant of proportionality in (7.2) is comparable with that measured in grid-stirred experiments. The differences are probably a result of the different turbulent structures in the present experiments, and recent measurements also show significant large-scale streaming motions in grid-stirred tanks (Drayton 1993) which we have not observed in the source-sink experiments. Thus, while we find a similar qualitative behaviour, our entrainment rates appear to be different in detail. Further analysis of the turbulence structure at high values of F would be necessary to resolve this question.

At low values of the forcing parameter F there is no significant vertical mixing and a stable density gradient exists throughout the tank. The motion produced by the sources and sinks is observed to be nearly two-dimensional, and to undergo a transition to a large-scale circulation after a period of several hours. Comparable experiments have been carried out in a thin layer of electrically conducting fluid by Sommeria (1986), who generated a set of two-dimensional vortices by the imposition of electric current at an array of points. The three-dimensional motions were suppressed by the imposition of a uniform magnetic field. Sommeria observed a reduction in the number of vortices with increasing strength of the magnetic field, eventually concentrating all the energy at the largest available scale. This large-scale motion is reminiscent of the flow observed here at low F , although Sommeria observed

changes in direction for weaker magnetic fields. He also noted that this circulation arose ‘spontaneously’, but does not give the timescale.

Related experiments have also been carried out by Colin de Verdiere (1980), who forced turbulence using a set of sources and sinks in the base of a rotating tank containing unstratified fluid. He reported observations of the decay of the vortices on a f -plane which did not show any transition to large scales. The reason why the vortices in this rotating experiment did not interact is that they are irrotational. As Hide (1968) showed, the flow from the sources to the sinks takes place in Ekman layers, and this motion is essentially disconnected to the motion within the vortices. Consequently, the vortices do not interact with each other in any direct sense and they remain strongly linked to the forcing scale.

In the present experiments the forcing arrangement was set up so that no net impulse or angular momentum was imparted to the fluid. Measurements of the velocity field showed that these conditions were achieved in practice. Nevertheless, at low F , a mean circulation was set up in the central region of the tank. Once it was established the sense of this circulation remained constant throughout the remainder of the experiment. In every case this corresponded to at least 50 circulation times. Both signs of circulation were observed and it seems probable that the direction resulted from some small bias in the arrangement of sources and sinks, which were altered slightly from one experiment to another. The mechanism for the rectification of the flow is not known, although once established it would deflect the jets from the sources in such a way as to enhance the circulation. Thus we believe it to be caused by nonlinear interaction between the jets and the circulation resulting from some initial instability. Furthermore, the strength of the circulation, as measured by the maximum velocity, was comparable with that of the flow from the sources. As a result of the no-slip condition it is, of course, the case that the total circulation around the boundary of the tank is zero. Consequently, the area integrals of the vorticity inside and outside a contour enclosing the circulation are equal and opposite. This result is consistent with the vorticity distributions shown in figure 14. The vorticity is negative everywhere within the circulation (figures 14*a* and 14*b*). Figure 14(*c*) shows the distribution around the circle $r = 0.75$ which is near the boundary of the circulation shown in figure 12. The vorticity outside the circulation ($r = 0.95$, shown in figure 14*d*) is almost all positive even though there is a strong inward flux of negative vorticity. The integral of the vorticity over the whole flow is approximately 1% of the peak value of ω , as expected.

The reduction in the number of vortices with time is similar to that observed in numerical calculations by McWilliams (1991), although in those calculations the flow was freely evolving from an initial vorticity distribution. In our experiments the flow continues to be forced, so that new vortices are generated within the interior of the flow domain. Despite these differences, evolution times in the two flows are quite similar, both taking about $200\tau_E$, where τ_E is the circulation timescale based on the initial eddy length and velocity scales. Recently, Dritschel (1993) has calculated the two-dimensional decay of patches of vorticity and found that as the system evolves the number of vortices increases with time. Vortices do coalesce by merging into a few large structures, but in the process large numbers of small-scale vortices are generated by the roll-up of vorticity filaments shed during the merging process. Dritschel’s calculations are effectively inviscid and so are not strictly relevant to our experimental parameter range where vortex Reynolds numbers are $\sim 10^3$ (see below). Furthermore, the spatial resolution of our measurements is not sufficient to detect such small-scale features of the flow.

The time evolution for small values of the forcing parameter F is consistent with the

'inverse energy cascade' of two-dimensional turbulence. For these highly stratified flows the motion is almost planar at all times. In the early stages of the flow the fluid above and below the forcing region is at rest and so there is significant vertical shear of the horizontal velocities. At later times this motion penetrates into these regions away from the forcing level either by stresses associated with dissipating internal waves or by viscous diffusion of momentum. Unfortunately, we have not examined this mechanism in detail although our video recordings do show some evidence of internal waves in the stratified regions. Equally, the timescale for viscous diffusion, based on the kinematic viscosity ν and the depth of the fluid, is about 5 hours which corresponds quite well with the establishment of the large-scale circulation (see figure 2). In any event, the vertical shear diminishes, the conditions for two-dimensionality are achieved and there is an accumulation of energy at the largest possible scale.

The end result is a flow of almost uniform vorticity within the large-scale circulation, and this appears to be an example of vorticity expulsion described by Batchelor (1956), and extended to turbulent flows by Rhines & Young (1982). Weak diffusion causes gradients of ω to vanish within closed ψ contours, and Rhines & Young (1982) show that expulsion occurs on two timescales. For high-Péclet-number flows there is a rapid phase caused by shear dispersion, followed by a diffusive phase. In our experiments the expulsion occurs on a timescale consistent with diffusion based on laminar viscosity, and it may be that at the Reynolds numbers achieved in the flow ($\sim 10^3$), based on eddy length and velocity scales) viscous effects are dominant over long times. This result is also consistent with the cascade of enstrophy to small scales and the subsequent dissipation of vorticity away from the region of direct influence of the forcing.

The slow decay of the unforced motion at low F is also consistent with the inverse energy cascade induced by the inhibition of vertical motions. When the flow is two-dimensional and steady there is a direct functional relationship between vorticity and streamfunction $\omega = \omega(\psi)$. A collapse of (ψ, ω) values onto a single curve is observed when the forcing ceases (figure 19) and we find an approximately linear relationship between ω and ψ . This relationship is similar to that found in the core of monopole vortices in a rotating fluid by Kloosterziel & van Heijst (1991). A linear relationship is also predicted by considerations of enstrophy decay leading to a monopole with minimum enstrophy (Leith 1984).

Another striking feature of the freely evolving vortex is the observed axisymmetrization. This property is a characteristic feature of free vortices and is discussed by Melander, McWilliams & Zabusky (1987). They argue that axisymmetrization may result from filamentation of the asymmetric vortex in an essentially inviscid process. While we observe a rapid transition to an axisymmetric flow in a timescale much shorter than the viscous decay time, we did not observe any filamentation. However, our spatial resolution may have been too coarse to resolve the filaments. McWilliams (1990) also points out that a general property of the transfer of energy to large scales implies that the flow will tend to the axisymmetric state as this has the largest scale. It would be interesting to see if this result holds in other domain shapes.

The results have been presented in terms of the two parameters $F = V/Nd$ and $Re = Vd/\nu$ based on the external variables controlling the flow. The flow evolves so that the diameter d of the sources and sinks appears to have little bearing on the flow structures. Using (7.1) and observations of the horizontal eddy scale, we can relate these parameters to the more natural internal Froude and Reynolds numbers based on the velocities and diameters of the eddies themselves. Typical values of the Reynolds numbers are $\sim 10^3$ which are not very large but are comparable with those achieved in

numerical calculations. We, therefore, expect the eddy interactions to be dominated by inertial processes, although viscous effects cannot be neglected entirely.

The values of the Froude number based on the initial value of N and on the eddy length and velocity scales are typically in the range 0.01–0.1. At the larger values vertical mixing reduces the value of N and hence the effective Froude number is larger still. Ocean eddies have Froude numbers $\sim 10^{-2}$, comparable with the strongly stratified flows here. Thus we expect them to cause little vertical mixing and for their dynamics to be controlled by the stratification. The reason that ocean eddies do not amalgamate into a single circulation results from the Coriolis force associated with the rotation of the Earth. An investigation of this effect will be the subject of a subsequent paper.

We designed these experiments in order to investigate the dynamics of stratified turbulence, particularly when the stratification is sufficiently strong to ensure that the turbulence is primarily two-dimensional. Our experiments have shown that it is possible to generate sufficiently energetic turbulence to produce vertical mixing at high Froude numbers, and to produce the desired two-dimensional motion at low Froude numbers. We have studied the various flow regimes, and investigated some of the dynamics. However, it soon became clear to us that the present experimental arrangement was very limited in one essential respect, namely the similarity between the forcing scale and the scale of the flow domain. Owing to the small number of sources and sinks we were only able to produce about ten vortices within the tank, and also the influence of each individual source extended to the middle of the flow domain. As a result we were unable to study the evolution of lengthscales in the flow to the extent we would have liked, and it was difficult to establish freely propagating vortices in the interior of the domain. We are currently investigating the flow produced by 40 source–sink pairs and the results of this work will be reported in a later paper.

REFERENCES

- BATCHELOR, G. K. 1956 Steady laminar flow with closed streamlines at large Reynolds number. *J. Fluid Mech.* **1**, 113–133.
- COLIN DE VERDIERE, A. 1980 Quasi-geostrophic turbulence in a rotating homogeneous fluid. *Geophys. Astrophys. Fluid Dyn.* **15**, 213–251.
- DALZIEL, S. B. 1993 Rayleigh–Taylor instability: experiments with image analysis. *Dyn. Atmos. Oceans* (in press).
- DRAYTON, M. J. 1993 Eulerian & Lagrangian studies of inhomogeneous turbulence generated by an oscillating grid. PhD thesis, University of Cambridge.
- DRITSCHEL, D. G. 1993 Vortex properties of two-dimensional turbulence. *Phys. Fluids A* **5**, 984–997.
- E, X. & HOPFINGER, E. J. 1986 On mixing across an interface in stably stratified fluid. *J. Fluid Mech.* **166**, 227–244.
- FERNANDO, H. J. S. 1991 Turbulent mixing in stratified fluids. *Ann. Rev. Fluid Mech.* **23**, 455–493.
- HEIJST, G. J. F. VAN & FLÓR, J. B. 1989 Dipole formation and collisions in a stratified fluid. *Nature* **340**, 212–215.
- HIDE, R. 1968 On source–sink flows in a rotating fluid. *J. Fluid Mech.* **32**, 737–764.
- KLOOSTERZIEL, R. C. & HEIJST, G. J. F. VAN 1991 An experimental study of unstable barotropic vortices in a rotating fluid. *J. Fluid Mech.* **223**, 1–24.
- LEGRAS, B., SANTANGELO, P. & BENZI, R. 1988 High resolution numerical experiments for forced two-dimensional turbulence. *Europhys. Lett.* **5**, 37–42.
- LEITH, C. E. 1984 Minimum enstrophy vortices. *Phys. Fluids* **27**, 1388–1395.
- MCWILLIAMS, J. C. 1984 The emergence of isolated coherent vortices in turbulent flow. *J. Fluid Mech.* **146**, 21–43.

- MCWILLIAMS, J. C. 1990 The vortices of two-dimensional turbulence. *J. Fluid Mech.* **219**, 361–385.
- MCWILLIAMS, J. C. 1991 Geostrophic vortices. In *Nonlinear Topics in Ocean Physics* (ed. A. R. Osborne), pp. 5–50. North Holland.
- MELANDER, M. V., MCWILLIAMS, J. C. & ZABUSKY, N. J. 1987 Axisymmetrization and vorticity-gradient intensification of an isolated two-dimensional vortex through filamentation. *J. Fluid Mech.* **178**, 137–159.
- NOKES, R. I. 1988 On the entrainment rate across a density interface. *J. Fluid Mech.* **188**, 185–204.
- READ, P. L., RHINES, P. B. & WHITE, A. A. 1986 Geostrophic scatter diagrams and potential vorticity dynamics. *J. Atmos. Sci.* **43**, 3226–3240.
- RHINES, P. B. & YOUNG, W. R. 1982 Homogenization of potential vorticity in planetary gyres. *J. Fluid Mech.* **122**, 347–367.
- RHINES, P. B. & YOUNG, W. R. 1983 How rapidly is a passive scalar mixed within closed streamlines? *J. Fluid Mech.* **133**, 133–145.
- SOMMERIA, J. 1986 Experimental study of the two-dimensional inverse energy cascade in a square box. *J. Fluid Mech.* **170**, 139–168.
- VORAPAYEV, S. I. 1989 Flat vortex structures in a stratified fluid. In *Mesoscale/synoptic Coherent Structures in Geophysical Turbulence* (ed. J. C. J. Nihoul & B. M. Jamart), pp. 671–689. Elsevier.